



AFRL-RZ-WP-TR-2010-2232

THE EFFECTS OF ORIENTATION AND ELEVATED ACCELERATION ON THE COOLING PERFORMANCE OF A CENTRIFUGE-MOUNTED SPRAY COOLING SYSTEM

Levi J. Elston

**Thermal and Electrochemical Branch
Energy/Power/Thermal Division**

**SEPTEMBER 2010
Interim Report**

Approved for public release; distribution unlimited.

See additional restrictions described on inside pages

STINFO COPY

**AIR FORCE RESEARCH LABORATORY
PROPULSION DIRECTORATE
WRIGHT-PATTERSON AIR FORCE BASE, OH 45433-7251
AIR FORCE MATERIEL COMMAND
UNITED STATES AIR FORCE**

NOTICE AND SIGNATURE PAGE

Using Government drawings, specifications, or other data included in this document for any purpose other than Government procurement does not in any way obligate the U.S. Government. The fact that the Government formulated or supplied the drawings, specifications, or other data does not license the holder or any other person or corporation; or convey any rights or permission to manufacture, use, or sell any patented invention that may relate to them.

This report was cleared for public release by the USAF 88th Air Base Wing (88 ABW) Public Affairs (AFRL/PA) Office and is available to the general public, including foreign nationals. Copies may be obtained from the Defense Technical Information Center (DTIC) (<http://www.dtic.mil>).

AFRL-RZ-WP-TR-2010-2232 HAS BEEN REVIEWED AND IS APPROVED FOR PUBLICATION IN ACCORDANCE WITH THE ASSIGNED DISTRIBUTION STATEMENT.

*//Signature//

LEVI ELSTON
Program Manager
Thermal and Electrochemical Branch
Energy/Power/Thermal Division

//Signature//

THOMAS L. REITZ
Chief, Thermal and Electrochemical Branch
Energy/Power/Thermal Division
Propulsion Directorate

This report is published in the interest of scientific and technical information exchange, and its publication does not constitute the Government's approval or disapproval of its ideas or findings.

*Disseminated copies will show “//Signature//” stamped or typed above the signature blocks.

REPORT DOCUMENTATION PAGE

*Form Approved
OMB No. 0704-0188*

The public reporting burden for this collection of information is estimated to average 1 hour per response, including the time for reviewing instructions, searching existing data sources, gathering and maintaining the data needed, and completing and reviewing the collection of information. Send comments regarding this burden estimate or any other aspect of this collection of information, including suggestions for reducing this burden, to Department of Defense, Washington Headquarters Services, Directorate for Information Operations and Reports (0704-0188), 1215 Jefferson Davis Highway, Suite 1204, Arlington, VA 22202-4302. Respondents should be aware that notwithstanding any other provision of law, no person shall be subject to any penalty for failing to comply with a collection of information if it does not display a currently valid OMB control number. **PLEASE DO NOT RETURN YOUR FORM TO THE ABOVE ADDRESS.**

1. REPORT DATE (DD-MM-YY) September 2010			2. REPORT TYPE Interim		3. DATES COVERED (From - To) 01 May 2009 – 31 August 2010	
4. TITLE AND SUBTITLE THE EFFECTS OF ORIENTATION AND ELEVATED ACCELERATION ON THE COOLING PERFORMANCE OF A CENTRIFUGE-MOUNTED SPRAY COOLING SYSTEM			5a. CONTRACT NUMBER In-house			
			5b. GRANT NUMBER			
			5c. PROGRAM ELEMENT NUMBER 62203F			
6. AUTHOR(S) Levi J. Elston			5d. PROJECT NUMBER 3145			
			5e. TASK NUMBER 22			
			5f. WORK UNIT NUMBER 314522B6			
7. PERFORMING ORGANIZATION NAME(S) AND ADDRESS(ES) Thermal and Electrochemical Branch (AFRL/RZPS) Energy/Power/Thermal Division Air Force Research Laboratory, Propulsion Directorate Wright-Patterson Air Force Base, OH 45433-7251 Air Force Materiel Command, United States Air Force			8. PERFORMING ORGANIZATION REPORT NUMBER AFRL-RZ-WP-TR-2010-2232			
			10. SPONSORING/MONITORING AGENCY ACRONYM(S) AFRL/RZPS			
9. SPONSORING/MONITORING AGENCY NAME(S) AND ADDRESS(ES) Air Force Research Laboratory Propulsion Directorate Wright-Patterson Air Force Base, OH 45433-7251 Air Force Materiel Command United States Air Force			11. SPONSORING/MONITORING AGENCY REPORT NUMBER(S) AFRL-RZ-WP-TR-2010-2232			
			12. DISTRIBUTION/AVAILABILITY STATEMENT Approved for public release; distribution unlimited.			
13. SUPPLEMENTARY NOTES PAO Case Number: 88ABW-2010-5234, Clearance Date: 28 Sep 2010. Report contains color.						
14. ABSTRACT A two-nozzle spray cooling system (R-134a) was installed on an 8-foot-diameter centrifuge table to test the effects of elevated acceleration on steady state cooling performance. Acceleration effects were evaluated in four orientations relative to the acceleration vector, which ranged from 1-10 g's. The 2-cm ² heated surface removed heat fluxes up to 250 W/cm ² in all test cases, and small performance improvements were seen at high accelerations in certain orientations. Additionally, the vertical spraying upward and horizontal spraying orientations demonstrated improved cooling over the nominal downward spraying orientation, with a decreasing effect as radial acceleration increased.						
15. SUBJECT TERMS spray cooling, centrifuge, acceleration, gravity, high heat flux, two-phase						
16. SECURITY CLASSIFICATION OF: a. REPORT Unclassified b. ABSTRACT Unclassified c. THIS PAGE Unclassified			17. LIMITATION OF ABSTRACT: SAR	18. NUMBER OF PAGES 64	19a. NAME OF RESPONSIBLE PERSON (Monitor) Levi J. Elston 19b. TELEPHONE NUMBER (Include Area Code) N/A	

Table of Contents

1. Introduction.....	1
2. Experimental Setup	2
2.1. RINI spray cooling system.....	2
2.1.1. Spray head	2
2.1.2. Reservoir.....	2
2.1.3. Condenser	3
2.1.4. Pump	3
2.2. Structural requirements	3
2.3. Acceleration and orientation adaptability	3
2.4. Centrifuge table integration, control, and monitoring	5
2.4.1. Power connection.....	5
2.4.2. Instrumentation/control connection	6
2.4.3. Cooling connection.....	6
2.4.4. Data acquisition system	6
2.5. Experimental Operation	7
2.5.1. Test objectives.....	8
2.5.2. Test operation	9
2.5.3. Data handling	9
2.6. Uncertainty and measurement error	9
2.6.1. Temperature measurement uncertainty	10
2.6.2. Pressure measurement uncertainty.....	11
2.6.3. Acceleration measurement uncertainty	11
2.6.4. Heat flux measurement uncertainty	11
2.7. Test parameters	12
3. Results & Discussion.....	13
3.1. Effect of Acceleration	15
3.1.1. Vertical Spraying Downward (VSD)	17
3.1.2. Vertical Spraying Upward (VSU)	18
3.1.3. Horizontal Spraying Outward (HSO).....	21
3.2. Effect of Orientation.....	23
4. Conclusions.....	27
5. Acknowledgements	28
6. Bibliography.....	29
Appendix A RINI Centrifuge Spray Cooling Experiment Standard Operation Procedure.....	30
Appendix B RINI Centrifuge Spray Cooling Experiment Standard Shutdown Procedure	31
Appendix C Acceleration vector alignment error	32
Appendix D Horizontal Spraying Inward (HSI).....	34
Appendix E Acceleration Calculation of the Heated Surface during Centrifuge Testing.....	35
Appendix F Structural Analysis	37
Appendix G Test Plan.....	45

List of Figures

Figure 1: Flow Loop Schematic For RINI Spray Cooling System And Glycol Based Chiller	2
Figure 2: A Picture Of The RINI Experimental Centrifuge Spray Cooling System	3
Figure 3: Acceleration Vector Error Experiment. The Plumb-Bob (White String) Angle Is Shown In Relation To The Angle Of The Reservoir In The 2g Test Case.....	4
Figure 4: Spray Head Nozzle (And Heated Surface) Orientation Relative To Acceleration Resultant Vector	5
Figure 5: Centrifuge Table Slip Ring Assembly: (a) Power Slip Rings; (b) Instrumentation Slip Rings	5
Figure 6: RINI Centrifuge ESC Labview Setup; (a) Control Screen, (b) Strip Chart And Steady State Operation Screen, (c) Flow Loop Schematic And Hand Record Data Screen	9
Figure 7: Sample Of Collected Data During 4g Acceleration (Orientation: Vertical Spraying Downward). Systematic Increase Of Heater Power Is Shown After Extended Steady State Operation ($a = 4.08 \pm 0.04 \text{ g}$, $T_{sat} = 22.15 \pm 0.12 \text{ }^{\circ}\text{C}$, $DP = 11.54 \pm 0.48 \text{ psid}$)	15
Figure 8: Acceleration Experienced On The Centrifuge Table: Left-Top View; Right-Side View....	16
Figure 9: Diagrams For The Four Evaluated Orientations Relative To Acceleration: (a) Vertical Spraying Downward; (b) Vertical Spraying Upward; (c) Horizontal Spraying Outward; (d) Horizontal Spraying Inward.	16
Figure 10: Steady State Cooling Performance For The Vertical Spraying Downward Orientation: (a) Heat Flux Vs. Surface Superheat; (b) Surface Superheat Vs. Acceleration ($T_{sat} = 22.66 \pm 2.33 \text{ }^{\circ}\text{C}$, $DP = 11.59 \pm 0.83 \text{ psid}$).	18
Figure 11: Steady State Cooling Performance For The Vertical Spraying Upward Orientation: (a) Heat Flux Vs. Surface Superheat; (b) Surface Superheat Vs. Acceleration ($T_{sat} = 23.82 \pm 2.85 \text{ }^{\circ}\text{C}$, $DP = 11.40 \pm 0.85 \text{ psid}$).	20
Figure 12: Steady State Cooling Performance For The Horizontal Spraying Outward Orientation: (a) Heat Flux Vs. Surface Superheat; (b) Surface Superheat Vs. Acceleration ($T_{sat} = 22.74 \pm 2.79 \text{ }^{\circ}\text{C}$, $DP = 11.76 \pm 0.76 \text{ psid}$).	22
Figure 13: Steady State Cooling Performance For The 1.05g Case, Heat Flux Vs. Surface Superheat ($a = 1.05 \pm 0.02 \text{ g}$, $T_{sat} = 22.93 \pm 2.91 \text{ }^{\circ}\text{C}$, $DP = 11.63 \pm 0.66 \text{ psid}$).	24
Figure 14: Steady State Cooling Performance For The 2g Case, Heat Flux Vs. Surface Superheat ($a = 2.04 \pm 0.04 \text{ g}$, $T_{sat} = 22.42 \pm 2.62 \text{ }^{\circ}\text{C}$, $DP = 11.53 \pm 0.62 \text{ psid}$).	24
Figure 15: Steady State Cooling Performance For The 4g Case, Heat Flux Vs. Surface Superheat ($a = 4.06 \pm 0.04 \text{ g}$, $T_{sat} = 23.16 \pm 3.11 \text{ }^{\circ}\text{C}$, $DP = 11.65 \pm 0.77 \text{ psid}$).	25
Figure 16: Steady State Cooling Performance For The 7g Case, Heat Flux Vs. Surface Superheat ($a = 7.06 \pm 0.06 \text{ g}$, $T_{sat} = 22.99 \pm 2.55 \text{ }^{\circ}\text{C}$, $DP = 11.51 \pm 1.20 \text{ psid}$).	25
Figure 17: Steady State Cooling Performance For The 10g Case, Heat Flux Vs. Surface Superheat ($a = 10.09 \pm 0.06 \text{ g}$, $T_{sat} = 23.51 \pm 2.70 \text{ }^{\circ}\text{C}$, $DP = 11.46 \pm 0.98 \text{ psid}$).	26
Figure 18: Acceleration Vector Alignment Error For 2g-10g Cases: (a) 2g=5.5°; (b) 3g=7.0°; (c) 4g=6.5°; (d) 5g=9.5°; (e) 6g=7.4°; (f) 7g=8.3°; (g) 8g=13.7°; (h) 9g=6.6°; (i) 10g=5.8°.	33
Figure 19: Steady State Cooling Performance For The Horizontal Spraying Inward Orientation: (a) Heat Flux Vs. Surface Superheat; (b) Surface Superheat Vs. Acceleration ($T_{sat} = 23.24 \pm 3.46 \text{ }^{\circ}\text{C}$, $DP = 11.50 \pm 0.96 \text{ psid}$).	34

List of Tables

Table 1: Instrument Quantity, Type, Range, And Accuracy	6
Table 2 Control Devices, Type, Range, And Expected Response Range.....	7
Table 3: Test Matrix For RINI Centrifuge Spray Cooling Experiment; Includes Orientation, Acceleration, Heat Flux, Logbook Information, And Data File Name.....	8
Table 4: Measurement Uncertainty Values.....	10
Table 5: Total (Measurement + Statistical) Uncertainty Values For A Sample Of Data Points For The 1.05g Case In The Vertical Spraying Downward Orientation	12
Table 6: RINI Centrifuge Spray Cooling Test Conditions.....	14

1. Introduction

As electronic devices increase in power and decrease in size, the heat removal requirements and difficulty increase significantly. Additionally, the presence of a variable body force environment (as seen on aircraft) imposes further challenges to high heat flux removal techniques. Spray cooling is one such technique that is capable of efficiently removing greater than 100 W/cm^2 in stable environments. Work has been conducted by NASA and the Air Force to investigate reduced (0.001g) and marginally-elevated (2.0g) gravity spray cooling performance in transient quasi-steady state operation. Tactical aircraft are capable of reaching much higher accelerations during maneuvers. These maneuvers can reach up to 10g's for short durations and are very transient in nature. As high power sensor suites and power conversion packages make their way towards aircraft integration, high heat flux cooling schemes such as spray cooling are expected to follow as an enabling technology for successful assimilation. To date no spray cooling experimental system has been evaluated in an elevated gravitational environment, whether it is a steady-state or an aircraft-like transient situation.

Significant effort has been completed in the area of spray cooling in non-terrestrial acceleration environments in recent years. Microgravity spray cooling using a single nozzle has been under investigation for some time (Yoshida, et al. 2001), showing inconclusive results. More recent research has demonstrated a trend of performance improvement with decreasing acceleration, on the range of 0.01 to 1.8g's in both single phase (Yerkes, et al. 2006) and two-phase(Michalak, et al. 2010) operation. Spray cooled arrays have been examined in micro-gravity environments (Elston, et al. 2009) where significant improvements in cooling performance were seen over terrestrial gravity, but chamber design may have been a strong contributing factor. Also, an analysis on the many factors that contribute to spray cooling performance for microgravity applications was completed, suggesting that test conditions, dissolved gasses, spray inclination angle, spray cooling enhancements (surfactants, grooves, and other surface structures), and impacts on film thickness can all have effects as significant as gravitational forces (Silk, Golliher and Selvam 2008).

Additionally, orientation effects have been shown to affect performance significantly. Testing using heated surfaces in vertical and horizontal (with nozzles spraying upward) orientations (all in bench-top tests: 1g) showed a 5% improvement in critical heat flux in the horizontal spraying upward case over the vertical case. Also, spray cooling modeling efforts have been completed studies in 0.0001-2.0g simulation environments (Selvam, et al. 2009), where very little effect from acceleration was seen on heat transfer. To date, no work has been found that has evaluated the effects of elevated gravity (up to 10 g's) on the cooling performance of an evaporative spray cooling array.

The transient nature of aircraft maneuvers inherently suggests testing a cooling system in an environment that closely mimics the acceleration profile of an F-15 or similar platform. As a first step in this direction, the goal of this effort was to evaluate a two-nozzle spray cooling system in elevated gravity (up to 10g) in a strictly steady-state operation, utilizing AFRL's Centrifuge Table Test Facility (Fleming 2010).

2. Experimental Setup

The two-nozzle centrifuge spray cooling experiment was designed, constructed, and tested (terrestrially only) by RINI Technologies as part of an Air Force Research Laboratory contract (FA8650-06-D-2620) funded via Congressional Interest Item. RINI Technologies utilized their high-heat flux spray cooling technologies in a closed loop cooling system. Structural and acceleration adaptability requirements were established for the system to be installed on AFRL's 8' diameter centrifuge table (ref Andy's paper). Remote control and monitoring was also configured to be able to safely run the experiments from a nearby control room.

2.1. RINI spray cooling system

The RINI Technologies high-heat flux spray cooling system uses R-134a as the primary working fluid and ultimately rejecting the heat to a glycol based chiller system. The spray cooling flow loop, as shown in Figure 1, consists of four major components: the spray head, reservoir, condenser, and pump.

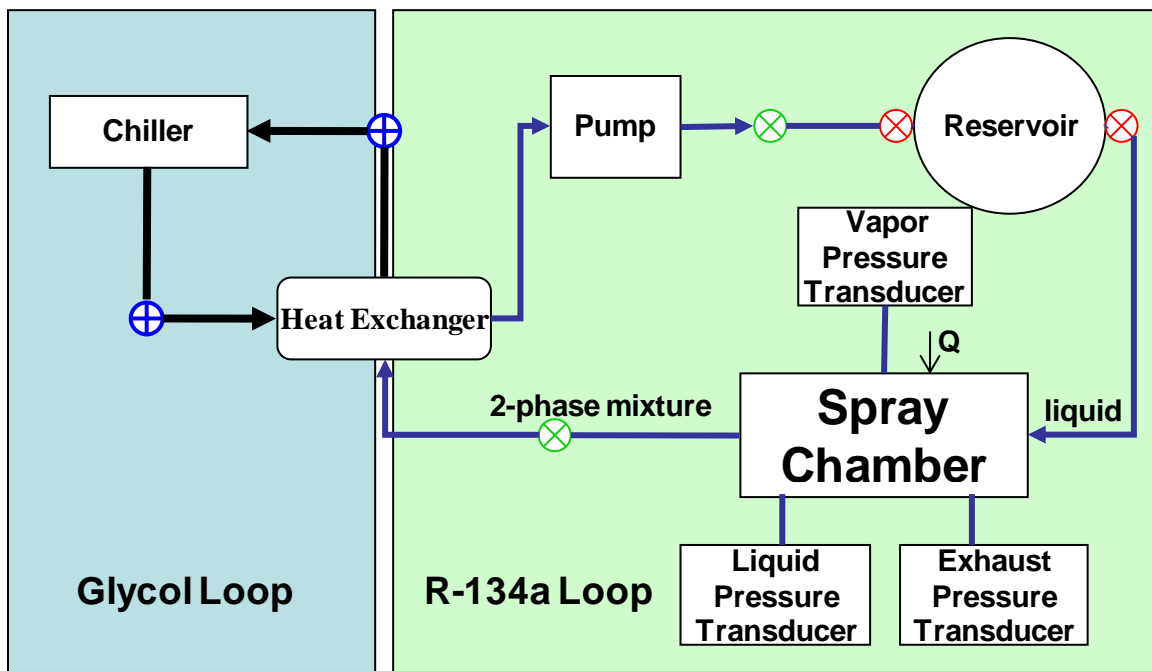


Figure 1: Flow Loop Schematic For RINI Spray Cooling System And Glycol Based Chiller

2.1.1. Spray head

The spray head consists of two-nozzles that cool a 2 cm^2 area heated by a thick-film resistance heater. The details of the spray head geometry contain proprietary information and are not discussed in this paper, but can be found in Distribution B AFRL Technical Report number AFRL-RZ-WP-TR-2009-2062.

2.1.2. Reservoir

The reservoir is approximately 0.6L in volume and is filled and pressurized by the pump. The pressurized reservoir then feeds saturated liquid from the bottom (explained in further detail in

section 2.3) to the spray chamber and ultimately the spray nozzles. In addition, the spray head is physically attached to the reservoir, as shown in Figure 2.

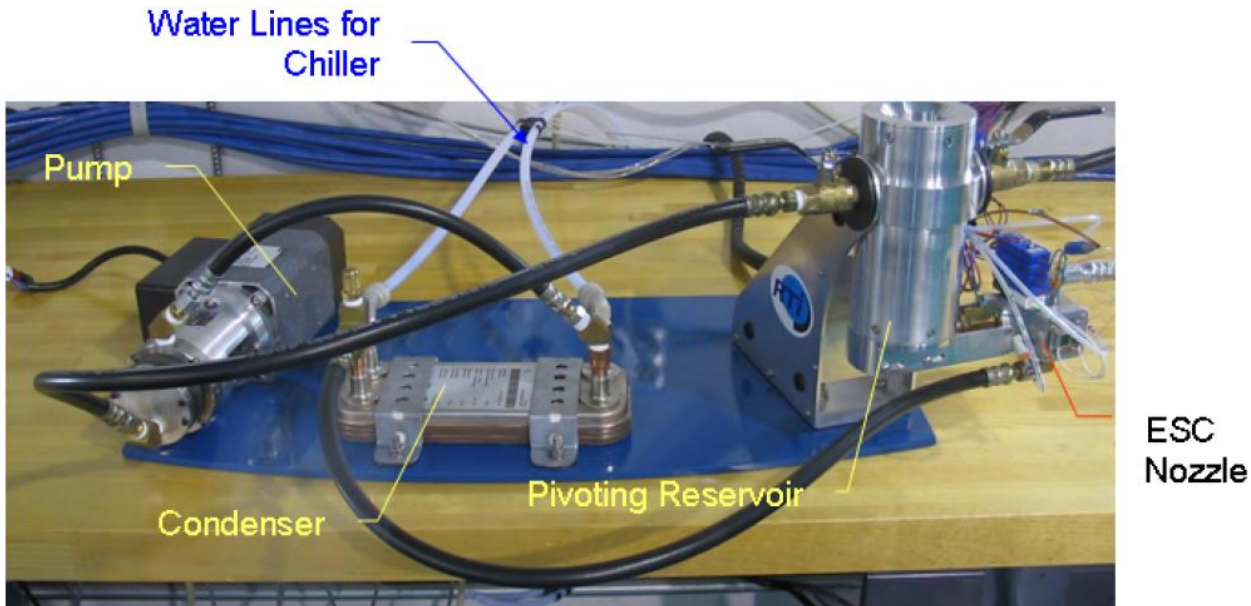


Figure 2: A Picture Of The RINI Experimental Centrifuge Spray Cooling System

2.1.3. Condenser

After the two-phase fluid exits the spray chamber, it enters the condenser which rejects heat to a glycol loop which is connected to an off-the-table chiller via a hydraulic coupling. The condenser is a Lytron heat exchanger made of stainless steel and is a commercial off-the-shelf item.

2.1.4. Pump

Lastly, the pump is a two-phase rotary-style prototype pump that is used to pull fluid from the condenser and fill/pressurize the reservoir. The pump has a remote variable speed control and therefore is able to maintain the required 10-12 psid (performance design condition) pressure drop across the nozzles throughout the 1-10g test matrix. The pump is also shown in Figure 2.

2.2. Structural requirements

The components associated with the 2-phase flow loop were required to undergo accelerations of 10g's with a factor of safety of 2 (20g's). All components were attached to an aluminum plate (oriented at a 4' radius) and were examined with an in-depth structural analysis. Appendix F includes further details regarding the structural analysis as provided by the contractor (RINI Technologies) prior to being installed on the centrifuge table.

2.3. Acceleration and orientation adaptability

An important requirement to properly conduct consistent acceleration vector tests required an adjustable spray nozzle head. RINI's spray head design was attached to a reservoir that is able to pivot to align itself with the acceleration vector. Figure 3 shows the reservoir and its orientation to the acceleration vector. Binding due to the plumbing and wiring associated with the spray head

created non-exact acceleration vector alignment. For this reason, the error in this vector was determined using a visual measurement technique. This technique involved the RINI flow loop mounted on the centrifuge table, a plumb-bob, and a high speed video camera. The centrifuge was spun at each acceleration (1g, 2g, 3g...10g) while the high-speed camera recorded images of the plumb-bob angle in relation to the reservoir angle. Figure 3 shows a frame taken from the 2g acceleration vector experiment. The error associated with the 2g case is estimated to be 5.5°. Additional information on the vector errors for 1-10g's are contained in Appendix C.

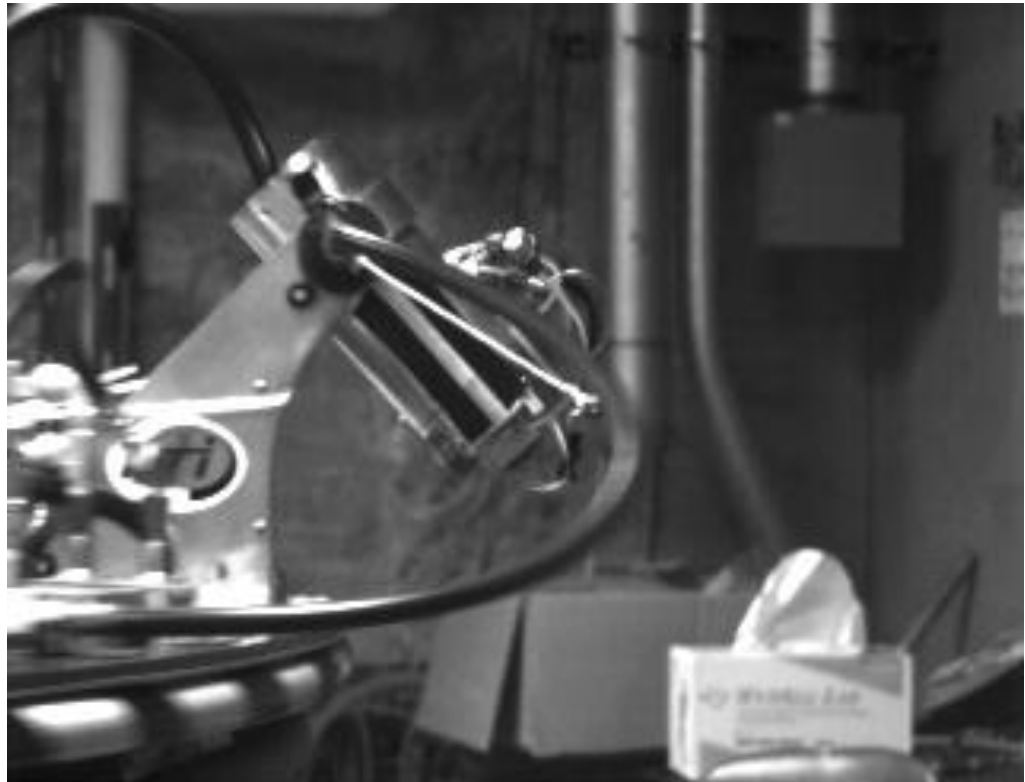


Figure 3: Acceleration Vector Error Experiment. The Plumb-Bob (White String) Angle Is Shown In Relation To The Angle Of The Reservoir In The 2g Test Case

In addition to acceleration vector alignment, the spray head was designed to change orientation relative to the acceleration vector, in 90° increments. The four orientations are (naming convention taken from no-spin, 1g condition): vertical spraying downward (spray in same direction as gravity), horizontal spraying outward (spray perpendicular to gravity), vertical spraying upward (spray in opposite direction as gravity), and horizontal spraying inward (spray perpendicular to gravity-similar effect expected as horizontal spraying outward condition). For radial accelerations above zero (table spinning), the acceleration resultant vector will be the combined 1g downward (due to gravity) and the radial acceleration pointing towards the center of the table (tangential acceleration ignored due to constant rotation speed during tests). The four orientations mentioned above, both vertical and one horizontal representation are displayed in Figure 4, were the basis for the testing. At each orientation, steady state data was taken for 0-250 W/cm² from 1-10g's.

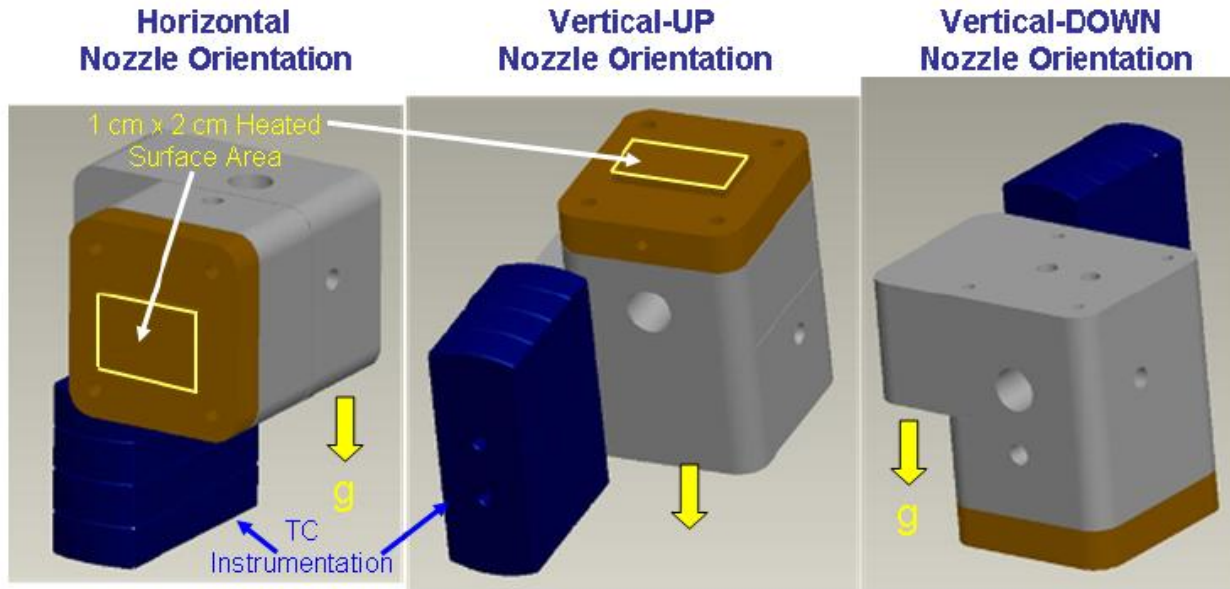


Figure 4: Spray Head Nozzle (And Heated Surface) Orientation Relative To Acceleration Resultant Vector

2.4. Centrifuge table integration, control, and monitoring

The RINI spray cooling system was installed on the centrifuge table by bolting the primary loop onto the outer edge of the 8' diameter table. The 3 primary connections between the RINI system and the AFRL centrifuge that needed to be made are: power, instrumentation/control, and cooling. Additionally, the control and data recording is completed by a data acquisition system.

2.4.1. Power connection

The 110VAC supply power for the pump and excitation power supplies passes through a set of large slip rings (see Figure 5(a)), from “off-table” to power the components “on-table”. Additionally, the DC power for the resistance heater (up to 500W) passes through another set of power slip rings. The heater power supply is “off-table” and is remotely controlled.

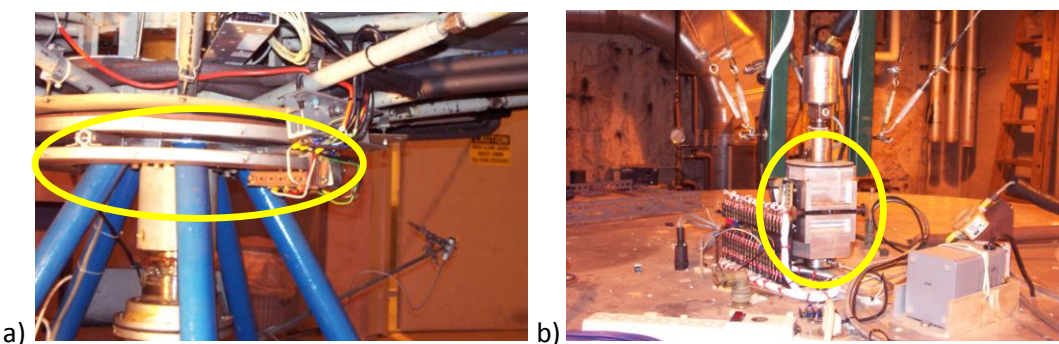


Figure 5: Centrifuge Table Slip Ring Assembly: (a) Power Slip Rings; (b) Instrumentation Slip Rings

2.4.2. Instrumentation/control connection

The low voltage instrumentation slip rings, as shown in Figure 5(b), are used to transfer data from the various thermocouples, pressure transducers, voltmeters, etc. to the data acquisition system that is located “off-table”. There are forty instrumentation channels available, but only sixteen channels were needed for data recording. Additionally, two more slip rings were used for the variable speed pump control.

2.4.3. Cooling connection

The heat removed via spray cooling was rejected to a glycol loop within the condenser. The glycol loop contained a primary chiller (with constant speed pump), a booster pump (to achieve higher flow rates), a flow-control valve (controlled via data acquisition system), and a hydraulic coupling at the centrifuge table interface to transfer the cold fluid onto the table and the warmed fluid back to the chiller. The glycol loop operated at 6-10° C and a flow rate range of 0.1-1.0 gpm to properly remove the heat from the spray cooling system (maintain a stable saturation pressure/temperature).

2.4.4. Data acquisition system

The data acquisition system consisted of an Agilent data acquisition chassis (with monitoring and control capability) and a standalone computer. The software was written using LabView and was used to record all data in addition to control. Table 1 shows the devices that were monitored during testing and their respective error and range of operation. Four thermocouples (type T) were placed within the heater assembly to monitor the surface temperature and distribution, one thermocouple (type T) was placed in the spray chamber to monitor saturation temperature, and the last two thermocouples (type T) were inserted in the inlet and outlet of the condenser (glycol loop side). The pressure transducers were plumbed to measure the nozzle liquid inlet pressure, chamber vapor pressure, and two-phase exhaust pressure. The flow meter was used to measure the flow rate of the glycol chiller loop. Lastly, the accelerometer was used to measure the acceleration in all three axes.

Table 1: Instrument Quantity, Type, Range, And Accuracy

Measurement	Sensor Type	Range	Accuracy
Thermocouples (7)	Thermocouples (Type T)	Calibrated (0-100 °C)	±0.62 °C
Pressure (3)	Pressure Transducers	Calibrated (0-100 psig)	±0.14 psig
Flow meter (1)	Piston	0-5 gpm	±0.125 gpm
Heater power (2)	Voltmeters (w/ precision resistor for current measurement)	0-500 W	±0.00025*V+0.005 (voltage measurement uncertainty)
Acceleration (1)	3-axis accelerometer	0-10 g	±0.01g
Accuracy assumes noiseless data (slip rings will increase these values)			

Table 2 shows the control devices used and their control ranges. The steady state acceleration was controlled via the electrical motor speed controller that was operated in the centrifuge control room. The nozzle pressure drop, with a design point of 10-12 psid, was controlled by the variable speed pump controller output from the data acquisition system (signal transferred through slip rings to “on-table” controller). Similarly, the flow rate was controlled with the data acquisition system output control. Additionally, for higher flow rate, the booster pump speed was adjusted using the pump

speed controller mounted inside the centrifuge table control room. Lastly, the heater power was adjusted using a low voltage signal from the data acquisition system to control the output power of the “off-table” heater power supply.

Table 2 Control Devices, Type, Range, And Expected Response Range

Control	Controller Type	Control Range	Response Range
Acceleration	Potentiometer Motor Controller	0-10 V	0-10 g's
Nozzle Pressure Drop (Pump Speed)	Computer D-A Output	0-5 V	0-15 psid
Ethylene Glycol Flow Rate (Chiller)	MFC-Computer D-A Output	4-20 mA	0-1 gpm
Heater Power	Computer D-A Output	0-5.25 V	0-500 W

2.5. Experimental Operation

The purpose of the testing was to generate high-g steady state testing of an evaporative spray cooling system. The testing will evaluate cooling performance as a function of acceleration (1-10 g's) and nozzle orientation (with respect to the acceleration vector). The metrics for successful testing include: acquiring accurate and stable data to build performance graphs (DT_{sat} vs. q'') as a function of the acceleration vector and nozzle orientation. The test matrix, shown in Table 3 took approximately one month to execute.

Table 3: Test Matrix For RINI Centrifuge Spray Cooling Experiment; Includes Orientation, Acceleration, Heat Flux, Logbook Information, And Data File Name

Test ID#	Nozzle Orientation	Acceleration	Heater Power (W)	Heat Flux (W/cm ²)	logbook	pg#	filename
RINI-1gvertdown	Vertical Spraying Down	1.01g	0-400 in 20 W increments	0-200 in 10 W/cm ² increments	00473	124	RINI Centrifuge ESC Wed, Jan 13, 2010, 0856
RINI-2gvertdown	Vertical Spraying Down	2g	0-400 in 20 W increments	0-200 in 10 W/cm ² increments	00473	123	RINI Centrifuge ESC Wed, Jan 13, 2010, 0658
RINI-3gvertdown	Vertical Spraying Down	3g	0-400 in 20 W increments	0-200 in 10 W/cm ² increments	00473	125	RINI Centrifuge ESC Wed, Jan 13, 2010, 1240
RINI-4gvertdown	Vertical Spraying Down	4g	0-400 in 20 W increments	0-200 in 10 W/cm ² increments	00473	126	RINI Centrifuge ESC Thu, Jan 14, 2010, 0708
RINI-5gvertdown	Vertical Spraying Down	5g	0-400 in 20 W increments	0-200 in 10 W/cm ² increments	00473	127	RINI Centrifuge ESC Thu, Jan 14, 2010, 0932
RINI-6gvertdown	Vertical Spraying Down	6g	0-400 in 20 W increments	0-200 in 10 W/cm ² increments	00473	128	RINI Centrifuge ESC Thu, Jan 14, 2010, 1158
RINI-7gvertdown	Vertical Spraying Down	7g	0-400 in 20 W increments	0-200 in 10 W/cm ² increments	00473	119	RINI Centrifuge ESC Mon, Jan 11, 2010, 1231
RINI-8gvertdown	Vertical Spraying Down	8g	0-400 in 20 W increments	0-200 in 10 W/cm ² increments	00473	117	RINI Centrifuge ESC Mon, Jan 11, 2010, 0715
RINI-9gvertdown	Vertical Spraying Down	9g	0-400 in 20 W increments	0-200 in 10 W/cm ² increments	00473	120	RINI Centrifuge ESC Tue, Jan 12, 2010, 0654
RINI-10gvertdown	Vertical Spraying Down	10g	0-400 in 20 W increments	0-200 in 10 W/cm ² increments	00473	121	RINI Centrifuge ESC Tue, Jan 12, 2010, 0943
RINI-1ghorizout	Horizontal Spraying Outward	1.01g	0-400 in 20 W increments	0-200 in 10 W/cm ² increments	00473	129	RINI Centrifuge ESC Tue, Jan 19, 2010, 0702
RINI-2ghorizout	Horizontal Spraying Outward	2g	0-400 in 20 W increments	0-200 in 10 W/cm ² increments	00473	130	RINI Centrifuge ESC Tue, Jan 19, 2010, 0940
RINI-3ghorizout	Horizontal Spraying Outward	3g	0-400 in 20 W increments	0-200 in 10 W/cm ² increments	00473	131	RINI Centrifuge ESC Tue, Jan 19, 2010, 1208
RINI-4ghorizout	Horizontal Spraying Outward	4g	0-400 in 20 W increments	0-200 in 10 W/cm ² increments	00473	132	RINI Centrifuge ESC Wed, Jan 20, 2010, 0703
RINI-5ghorizout	Horizontal Spraying Outward	5g	0-400 in 20 W increments	0-200 in 10 W/cm ² increments	00473	133	RINI Centrifuge ESC Wed, Jan 20, 2010, 1225
RINI-6ghorizout	Horizontal Spraying Outward	6g	0-400 in 20 W increments	0-200 in 10 W/cm ² increments	00473	134	RINI Centrifuge ESC Thu, Jan 21, 2010, 0719
RINI-7ghorizout	Horizontal Spraying Outward	7g	0-400 in 20 W increments	0-200 in 10 W/cm ² increments	00473	135	RINI Centrifuge ESC Thu, Jan 21, 2010, 0947
RINI-8ghorizout	Horizontal Spraying Outward	8g	0-400 in 20 W increments	0-200 in 10 W/cm ² increments	00473	136	RINI Centrifuge ESC Thu, Jan 21, 2010, 1230
RINI-9ghorizout	Horizontal Spraying Outward	9g	0-400 in 20 W increments	0-200 in 10 W/cm ² increments	00473	137	RINI Centrifuge ESC Fri, Jan 22, 2010, 0657
RINI-10ghorizout	Horizontal Spraying Outward	10g	0-400 in 20 W increments	0-200 in 10 W/cm ² increments	00473	138	RINI Centrifuge ESC Fri, Jan 22, 2010, 1224
RINI-1gvertup	Vertical Spraying Up	1.01g	0-400 in 20 W increments	0-200 in 10 W/cm ² increments	00473	139	RINI Centrifuge ESC Tue, Jan 26, 2010, 0844
RINI-2gvertup	Vertical Spraying Up	2g	0-400 in 20 W increments	0-200 in 10 W/cm ² increments	00473	140	RINI Centrifuge ESC Wed, Jan 27, 2010, 0704
RINI-3gvertup	Vertical Spraying Up	3g	0-400 in 20 W increments	0-200 in 10 W/cm ² increments	00473	141	RINI Centrifuge ESC Wed, Jan 27, 2010, 1238
RINI-4gvertup	Vertical Spraying Up	4g	0-400 in 20 W increments	0-200 in 10 W/cm ² increments	00473	142	RINI Centrifuge ESC Thu, Jan 28, 2010, 0640
RINI-5gvertup	Vertical Spraying Up	5g	0-400 in 20 W increments	0-200 in 10 W/cm ² increments	00473	143	RINI Centrifuge ESC Thu, Jan 28, 2010, 0914
RINI-6gvertup	Vertical Spraying Up	6g	0-400 in 20 W increments	0-200 in 10 W/cm ² increments	00473	144	RINI Centrifuge ESC Thu, Jan 28, 2010, 1201
RINI-7gvertup	Vertical Spraying Up	7g	0-400 in 20 W increments	0-200 in 10 W/cm ² increments	00473	145	RINI Centrifuge ESC Fri, Jan 29, 2010, 0639
RINI-8gvertup	Vertical Spraying Up	8g	0-400 in 20 W increments	0-200 in 10 W/cm ² increments	00473	148	RINI Centrifuge ESC Mon, Feb 01, 2010, 0657
RINI-9gvertup	Vertical Spraying Up	9g	0-400 in 20 W increments	0-200 in 10 W/cm ² increments	00473	149	RINI Centrifuge ESC Mon, Feb 01, 2010, 1210
RINI-10gvertup	Vertical Spraying Up	10g	0-400 in 20 W increments	0-200 in 10 W/cm ² increments	00473	150	RINI Centrifuge ESC Tue, Feb 02, 2010, 0725
RINI-1ghorizin	Horizontal Spraying Inward	1.01g	0-400 in 20 W increments	0-200 in 10 W/cm ² increments	00473	152	RINI Centrifuge ESC Wed, Feb 03, 2010, 0654
RINI-2ghorizin	Horizontal Spraying Inward	2g	0-400 in 20 W increments	0-200 in 10 W/cm ² increments	PR00025	25	RINI Centrifuge ESC Wed, Feb 03, 2010, 1216
RINI-3ghorizin	Horizontal Spraying Inward	3g	0-400 in 20 W increments	0-200 in 10 W/cm ² increments	PR00025	26	RINI Centrifuge ESC Thu, Feb 04, 2010, 0645
RINI-4ghorizin	Horizontal Spraying Inward	4g	0-400 in 20 W increments	0-200 in 10 W/cm ² increments	PR00025	27	RINI Centrifuge ESC Thu, Feb 04, 2010, 0938
RINI-5ghorizin	Horizontal Spraying Inward	5g	0-400 in 20 W increments	0-200 in 10 W/cm ² increments	PR00025	28	RINI Centrifuge ESC Fri, Feb 05, 2010, 0649
RINI-6ghorizin	Horizontal Spraying Inward	6g	0-400 in 20 W increments	0-200 in 10 W/cm ² increments	PR00025	29	RINI Centrifuge ESC Fri, Feb 05, 2010, 1229
RINI-7ghorizin	Horizontal Spraying Inward	7g	0-400 in 20 W increments	0-200 in 10 W/cm ² increments	PR00025	30	RINI Centrifuge ESC Mon, Feb 08, 2010, 0646
RINI-8ghorizin	Horizontal Spraying Inward	8g	0-400 in 20 W increments	0-200 in 10 W/cm ² increments	PR00025	31	RINI Centrifuge ESC Mon, Feb 08, 2010, 1215
RINI-9ghorizin	Horizontal Spraying Inward	9g	0-400 in 20 W increments	0-200 in 10 W/cm ² increments	PR00025	32	RINI Centrifuge ESC Tue, Feb 09, 2010, 0721
RINI-10ghorizin	Horizontal Spraying Inward	10g	0-400 in 20 W increments	0-200 in 10 W/cm ² increments	PR00025	33	RINI Centrifuge ESC Tue, Feb 09, 2010, 1000

2.5.1. Test objectives

The primary objective of this test was to determine the effect of body forces (and body force orientation) on the cooling performance of a 2-nozzle (with a 2 cm² heated surface) evaporative spray cooling (ESC) system. To properly measure this objective, the tests controlled and acquired the following data:

Control: table spin speed (acceleration), refrigerant flow rate (nozzle pressure drop), heater power (heat removed by ESC), and chiller flow rate (to maintain a stable saturation temperature).

Acquire: 4 temperatures in heater block (between heater and spray surface), saturation temperature in spray chamber, condenser temperature (chiller side), nozzle pressure, chamber pressure, acceleration, heater voltage, heater current.

A baseline for comparison was done before delivery of the system in 2007 (completed at contractor's facilities). This was used to compare the 1-g data to check for accuracy and hardware issues.

2.5.2. Test operation

The test was operated by first setting a nozzle orientation, then acceleration, a desired saturation temperature, and nozzle pressure drop. During a test, the orientation and acceleration remained constant while the heat input to the system was systematically adjusted (0-500 W in 20 W increments). During the test, the saturation temperature was held constant by controlling the chiller flow rate controls (mass flow controller and booster pump). After the system reaches a steady-state at a given data point, approximately 100 data points were recorded for further data reduction (1 data point was hand recorded at each steady state portion, sample hand recording sheet is appended). Each of these tests generated a performance curve at a given acceleration and nozzle orientation which will be discussed in Section 3.

2.5.3. Data handling

The display used during testing is shown in Figure 6. The LabView Front Panel was split up over 3 screens. The first screen (Figure 6(a)) was dedicated solely to control with some feedback associated with these controls. The second screen (Figure 6(b)) shows 4 strip charts that were used for indication as well as steady state determination. The third and final screen (Figure 6(c)) displays the simplistic flow loop schematics, specific thermocouple and pressure data, and a chart that lists the data for hand recording during the testing.

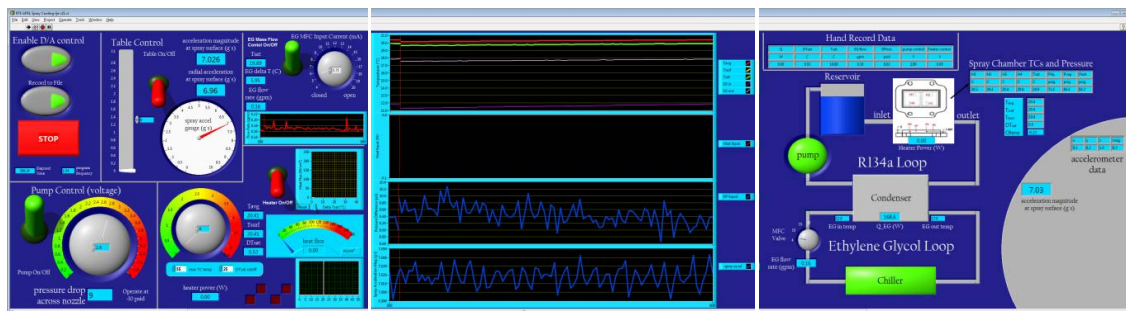


Figure 6: RINI Centrifuge ESC Labview Setup; (a) Control Screen, (b) Strip Chart And Steady State Operation Screen, (c) Flow Loop Schematic And Hand Record Data Screen

After all data was collected in a .txt format, it was converted to an Excel (.xlsx) file format for further data reduction.

2.6. Uncertainty and measurement error

The uncertainty in the recorded values is comprised of two components: measurement error and statistical error. For values that require only one measurement, such as pressure (uses only a pressure transducer), the measurement error is strictly associated with the device's calibration, as

shown in Table 1. For those values that require more than one measurement, such as DT_{sat} (uses five separate thermocouples), an uncertainty analysis must be conducted, and is shown in Sections 2.6.1-2.6.4. A summary of the measurement uncertainty results are shown in Table 4.

Table 4: Measurement Uncertainty Values

Measurement	Instrument error	Units
T (each thermocouple)	0.62	°C
DT_{sat}	0.627	°C
Heat flux	0.000356	W/cm ²
	3.56	W/m ²
Acceleration	0.01	g
	0.0981	m/s ²

The statistical error can also be a significant factor in the measured uncertainty. Since each of the conditions in the test matrix, as shown in Table 3, were taken in steady state, there was approximately 100 values recorded during that test condition. These 100 values were then averaged, which allowed for a statistical distribution for that average. The statistical error reported in this paper is calculated as \pm two standard deviations from the average value, which captures 95% of the data. The statistical error is then combined with the measurement error to report a total error. Due to the nature of transmitting power and data signals via the slip rings and slow-moving brushes, the statistical error was higher than a bench-top experiment would have produced. A sample data set displaying the total error (statistical and measurement) is shown in Table 5.

2.6.1. Temperature measurement uncertainty

Thermocouples were calibrated using a precision RTD and calibration bath on the range of 0-100 °C. The maximum uncertainty associated with this calibration was determined to be 0.62 °C. Additionally, the uncertainty analysis for DT_{sat} is shown below. T_1 , T_2 , T_3 , and T_4 are the thermocouples within the heater surface. The average of these values gives the average heater surface temperature.

$$DT_{sat} = T_{surf} - T_{sat} = \frac{T_1 + T_2 + T_3 + T_4}{4} - T_{sat}$$

$$\delta DT_{sat} = DT_{sat} \sqrt{\left[\frac{T_1}{DT_{sat}} \left(\frac{\partial DT_{sat}}{\partial T_1} \right) \frac{dT_1}{T_1} \right]^2 + \left[\frac{T_2}{DT_{sat}} \left(\frac{\partial DT_{sat}}{\partial T_2} \right) \frac{dT_2}{T_2} \right]^2 + \left[\frac{T_3}{DT_{sat}} \left(\frac{\partial DT_{sat}}{\partial T_3} \right) \frac{dT_3}{T_3} \right]^2 + \left[\frac{T_4}{DT_{sat}} \left(\frac{\partial DT_{sat}}{\partial T_4} \right) \frac{dT_4}{T_4} \right]^2 + \left[\frac{T_{sat}}{DT_{sat}} \left(\frac{\partial DT_{sat}}{\partial T_{sat}} \right) \frac{dT_{sat}}{T_{sat}} \right]^2}$$

$$\frac{\partial DT_{sat}}{\partial T_1} = \frac{1}{4} \quad dT_1 = 0.181 \text{ °C (from calibration)}$$

$$\begin{aligned}
\frac{\partial DT_{sat}}{\partial T_1} &= \frac{1}{4} & dT_2 &= 0.181 \text{ } ^\circ\text{C (from calibration)} \\
\frac{\partial DT_{sat}}{\partial T_1} &= \frac{1}{4} & dT_3 &= 0.185 \text{ } ^\circ\text{C (from calibration)} \\
\frac{\partial DT_{sat}}{\partial T_1} &= \frac{1}{4} & dT_4 &= 0.190 \text{ } ^\circ\text{C (from calibration)} \\
\frac{\partial DT_{sat}}{\partial T_1} &= -1 & dT_{sat} &= 0.62 \text{ } ^\circ\text{C (from calibration)}
\end{aligned}$$

$$\begin{aligned}
\delta DT_{sat} &= \sqrt{\left[\left(\frac{1}{4}\right) dT_1\right]^2 + \left[\left(\frac{1}{4}\right) dT_2\right]^2 + \left[\left(\frac{1}{4}\right) dT_3\right]^2 + \left[\left(\frac{1}{4}\right) dT_4\right]^2 + [(-1)dT_{sat}]^2} \\
\delta DT_{sat} &= \sqrt{\left[\left(\frac{1}{4}\right) 0.181\right]^2 + \left[\left(\frac{1}{4}\right) 0.181\right]^2 + \left[\left(\frac{1}{4}\right) 0.185\right]^2 \\
&\quad + \left[\left(\frac{1}{4}\right) 0.190\right]^2 + [(-1)0.62]^2} = 0.627 \text{ } ^\circ\text{C}
\end{aligned}$$

2.6.2. Pressure measurement uncertainty

The pressure transducers were calibrated using a precision pressure calibrator on the range of 0-100 psig. The accuracy of this calibration was determined to be 0.14 psig.

2.6.3. Acceleration measurement uncertainty

The uncertainty of the measured acceleration of the accelerometer is 0.01 g.

2.6.4. Heat flux measurement uncertainty

The heater flux was measured using 2 voltmeters and the heater area. The first voltmeter (V_1) was used to measure the voltage drop across the heater itself, where the second voltmeter (V_2) was used to measure the voltage drop across an inline precision resistor (0.1 ohms) which determines the current flow. The uncertainty in this measurement is shown below.

$$\begin{aligned}
q'' &= \frac{Q}{A} = \frac{VI}{A} = \frac{V_1 V_2}{AR} \\
\delta q'' &= q'' \sqrt{\left[\left(\frac{\partial q''}{\partial V_1}\right) \frac{dV_1}{q''}\right]^2 + \left[\left(\frac{\partial q''}{\partial V_2}\right) \frac{dV_2}{q''}\right]^2 + \left[\left(\frac{\partial q''}{\partial R}\right) \frac{dR}{q''}\right]^2 + \left[\left(\frac{\partial q''}{\partial A}\right) \frac{dA}{q''}\right]^2} \\
\delta q'' &= \sqrt{\left[\left(\frac{\partial q''}{\partial V_1}\right) dV_1\right]^2 + \left[\left(\frac{\partial q''}{\partial V_2}\right) dV_2\right]^2 + \left[\left(\frac{\partial q''}{\partial R}\right) dR\right]^2 + \left[\left(\frac{\partial q''}{\partial A}\right) dA\right]^2}
\end{aligned}$$

$$\frac{\partial q''}{\partial V_1} = \frac{V_2}{AR} \quad dV_1 = 0.00025V_1 + 0.005 \text{ V}$$

$$\frac{\partial q''}{\partial V_2} = \frac{V_1}{AR} \quad dV_2 = 0.00025V_2 + 0.005 \text{ V}$$

$$\frac{\partial q''}{\partial R} = -\frac{V_1 V_2}{AR^2} \quad dR = \pm 0.00002 \text{ } \Omega$$

$$\frac{\partial q''}{\partial A} = -\frac{V_1 V_2}{A^2 R} \quad dA = \sqrt{2[(2L)dL]^2} = \sqrt{2[(2 * .01).0001]^2} = 2.83e-6$$

$$\delta q'' = q'' \sqrt{\left[\frac{AR}{V_1 V_2} \left(\frac{V_2}{AR} \right) dV_1 \right]^2 + \left[\frac{AR}{V_1 V_2} \left(\frac{V_1}{AR} \right) dV_2 \right]^2 + \left[\frac{AR}{V_1 V_2} \left(-\frac{V_1 V_2}{AR^2} \right) dR \right]^2 + \left[\frac{AR}{V_1 V_2} \left(-\frac{V_1 V_2}{A^2 R} \right) dA \right]^2}$$

$$\delta q'' = q'' \sqrt{\left[\frac{dV_1}{V_1} \right]^2 + \left[\frac{dV_2}{V_2} \right]^2 + \left[-\frac{dR}{R} \right]^2 + \left[-\frac{dA}{A} \right]^2}$$

$$= q'' \sqrt{\left[\frac{0.00025 * V_1 + 0.005}{V_1} \right]^2 + \left[\frac{0.00025 * V_2 + 0.005}{V_2} \right]^2 + \left[-\frac{0.00002}{R} \right]^2 + \left[-\frac{2.83e - 6}{A} \right]^2}$$

$$\delta q'' \left(q'' = 250 \frac{W}{cm^2} \right)$$

$$= 2.5e^6 \sqrt{\left[\frac{2.5e^{-4} * 70.063 + 0.005}{70.063} \right]^2 + \left[\frac{2.5e^{-4} * 71.736 + 0.005}{71.736} \right]^2 + \left[-\frac{2.0e^{-5}}{0.1} \right]^2 + \left[-\frac{2.83e^6}{0.0002} \right]^2}$$

$$\delta q'' \left(q'' = 250 \frac{W}{cm^2} \right) = 3.56e - 4 \frac{W}{cm^2}$$

Table 5: Total (Measurement + Statistical) Uncertainty Values For A Sample Of Data Points For The 1.05g Case In The Vertical Spraying Downward Orientation

Sample data point # (for VSD 1.05g test)	DTsat (°C)		Heat Flux (W/cm ²)		Acceleration (g)	
	average	total error	average	total error	average	total error
6	8.93	0.886	49.51	2.36	1.057	0.025
10	10.74	0.823	89.85	2.51	1.056	0.053
14	12.83	0.795	129.11	2.96	1.056	0.031
18	15.92	0.805	169.04	3.00	1.058	0.023
22	19.89	0.825	210.05	2.93	1.057	0.023
26	24.40	0.906	249.84	3.44	1.056	0.030

2.7. Test parameters

The three parameters that were varied throughout the course of the testing were orientation, acceleration (a), and heat flux (q''). For each test condition, the system was held at steady state while the data acquisition system acquired approximately 100 data points. The nozzle was first oriented in the “vertical spraying downward” orientation and tested at 1-10g’s (0-250 W/cm² at each acceleration) before the orientation was subsequently changed to “horizontal spraying outward”, “vertical spraying upward”, and lastly “horizontal spraying inward” where 1-10g’s (0-250 W/cm² at each acceleration) was completed for each. The saturation temperature and nozzle pressure drop were held relatively constant for all tests through the use of adjustments in the chiller flow rate (increased as heater power increased) and two-phase pump speed, respectively.

3. Results & Discussion

The objective of the RINI centrifuge spray cooling system was to independently show the effects of elevated gravity and orientation to acceleration on spray cooling performance. As a means to simplifying the analysis, each test case, shown in Table 6, was defined independently by: orientation and acceleration. Each of these cases allowed only the heater power to vary. By doing this, heat transfer curves could easily be assembled under constant operating conditions.

An example data set, shown in Figure 7, depicts a portion of the data collected at 4 g's (orientation: vertical spraying downward) for step increases in heat flux. The acceleration magnitude, constant at 4g, is shown towards the bottom of the plot as the green flat line. The purple line shows the saturation temperature, T_{sat} , and demonstrates constant operation due to chiller flow rate control. The heat flux, shown with the blue line, demonstrates the stepwise operation of the tests. In Figure 7 the heat flux is increased from 170 W/cm² to 200 W/cm² in 10 W/cm² increments. Each step is maintained at a constant heat flux for approximately 180 s to reach a definite steady state condition. The DT_{sat} ($DT_{sat} = T_{surf} - T_{sat}$) curve, shown in red, reflects the steady state condition at each heat flux step. The system's steady state determination is made from the DT_{sat} line, which shows steady state being reached very quickly, allowing for greater than 100 s of steady state data point collection.

Table 6: RINI Centrifuge Spray Cooling Test Conditions

test case #	orientation	acceleration
1	vertical spraying downward	1.01g
2	vertical spraying downward	2g
3	vertical spraying downward	3g
4	vertical spraying downward	4g
5	vertical spraying downward	5g
6	vertical spraying downward	6g
7	vertical spraying downward	7g
8	vertical spraying downward	8g
9	vertical spraying downward	9g
10	vertical spraying downward	10g
11	horizontal spraying outward	1.01g
12	horizontal spraying outward	2g
13	horizontal spraying outward	3g
14	horizontal spraying outward	4g
15	horizontal spraying outward	5g
16	horizontal spraying outward	6g
17	horizontal spraying outward	7g
18	horizontal spraying outward	8g
19	horizontal spraying outward	9g
20	horizontal spraying outward	10g
21	vertical spraying upward	1.01g
22	vertical spraying upward	2g
23	vertical spraying upward	3g
24	vertical spraying upward	4g
25	vertical spraying upward	5g
26	vertical spraying upward	6g
27	vertical spraying upward	7g
28	vertical spraying upward	8g
29	vertical spraying upward	9g
30	vertical spraying upward	10g
31	horizontal spraying inward	1.01g
32	horizontal spraying inward	2g
33	horizontal spraying inward	3g
34	horizontal spraying inward	4g
35	horizontal spraying inward	5g
36	horizontal spraying inward	6g
37	horizontal spraying inward	7g
38	horizontal spraying inward	8g
39	horizontal spraying inward	9g
40	horizontal spraying inward	10g

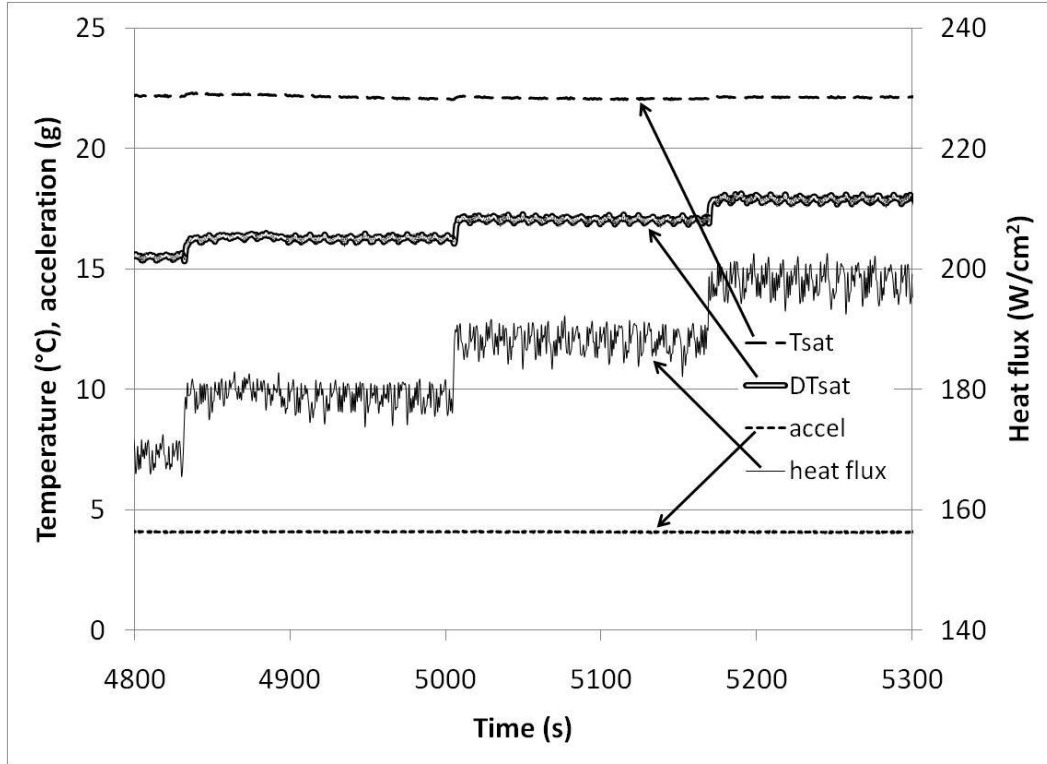


Figure 7: Sample Of Collected Data During 4g Acceleration (Orientation: Vertical Spraying Downward). Systematic Increase Of Heater Power Is Shown After Extended Steady State Operation ($a = 4.08 \pm 0.04$ g, $T_{sat} = 22.15 \pm 0.12$ °C, $DP = 11.54 \pm 0.48$ psid)

3.1. Effect of Acceleration

The tests were conducted at 1-10g's in 1g increments for each of four orientations. This section will discuss the results of the effect of acceleration on each orientation. The nominal case, vertical spraying downward, will be discussed first, followed by the vertical spraying upward, horizontal spraying outward, and horizontal spraying inward cases. Figure 9 shows the orientation of the spray and heated surface relative to the acceleration vector. Each of the orientation tests are represented by an acceleration magnitude that is the resultant of the radial acceleration and the acceleration due to gravity, as shown in Figure 8.

The following description of the orientations applies to the no-spin condition, as the radial acceleration increases, the acceleration resultant relative to the spray surface changes. For the "vertical spraying downward" case (Figure 9 (a)) gravity is normal to the heated surface and in the same direction as the spray. In the "vertical spraying upward" case (Figure 9 (b)) gravity is also normal to the heated surface, but in the opposite direction of the imparting spray. The "horizontal spraying outward" and "horizontal spraying inward" cases (Figure 9 (a) & (b)) are oriented such that gravity is parallel to the heated surface and perpendicular to the spray. It is also worth noting that the acceleration on the droplets having left the nozzle are undergoing strictly 1g downward (due to gravity) at all spin speeds. Only once the droplets have reached the surface and coalesce into the thin film is an effect due to radial acceleration experienced. Additionally, only 1.05g, 2g, 4g, 6g, 8g, and 10g data is shown to reduce the number of data traces on the plot for improved readability.

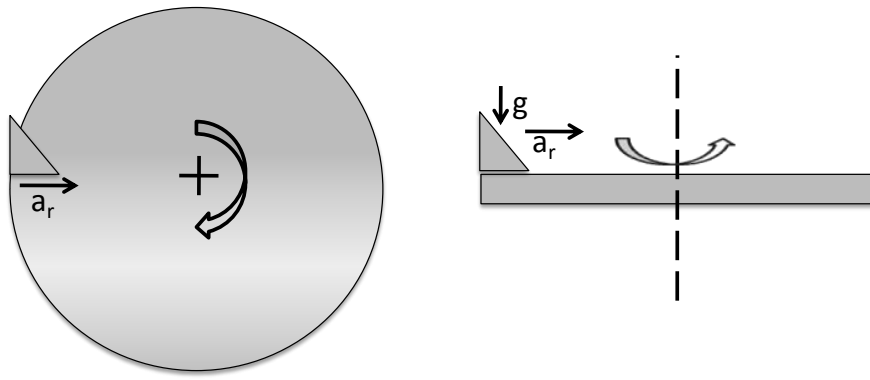


Figure 8: Acceleration Experienced On The Centrifuge Table: Left-Top View; Right-Side View

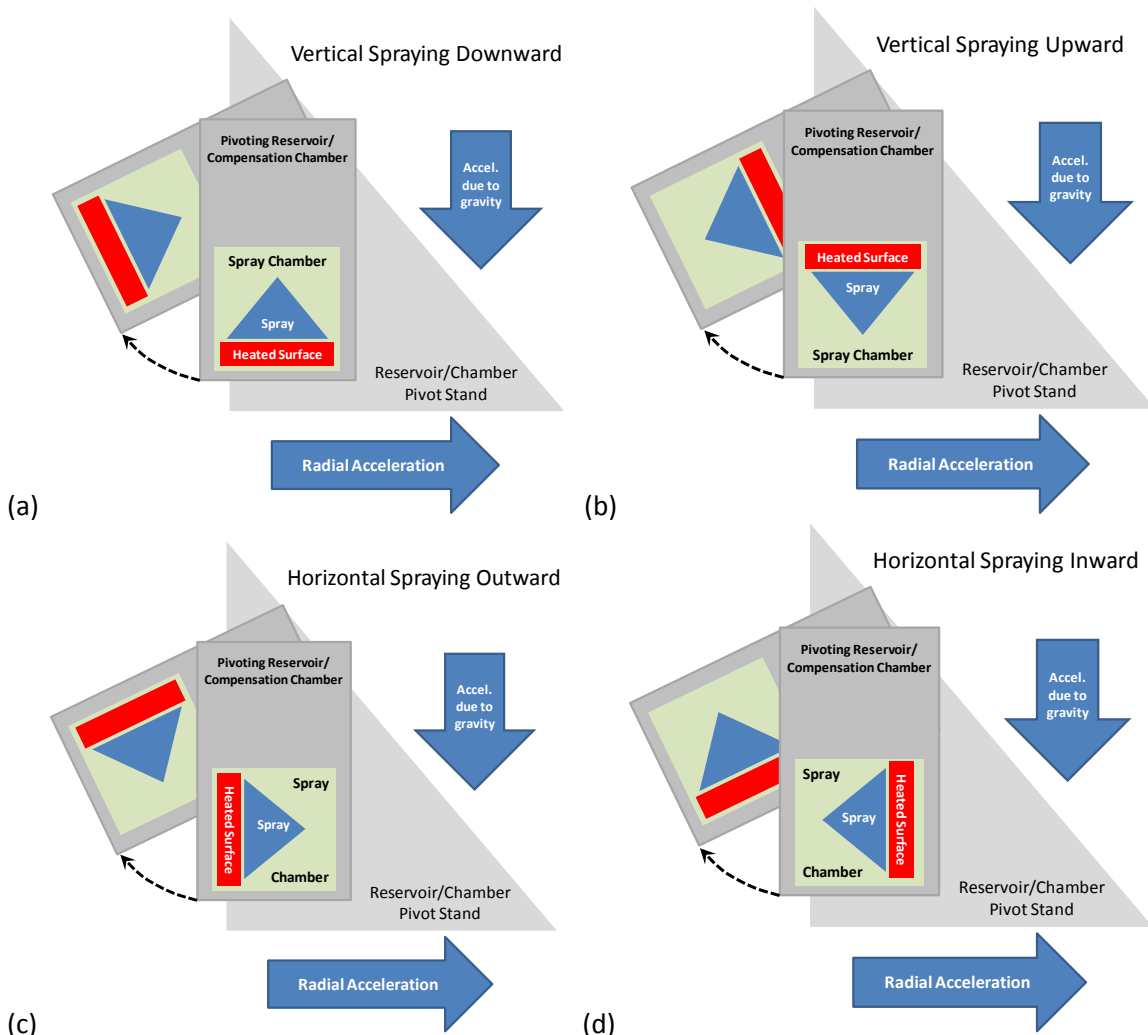


Figure 9: Diagrams For The Four Evaluated Orientations Relative To Acceleration: (a) Vertical Spraying Downward; (b) Vertical Spraying Upward; (c) Horizontal Spraying Outward; (d) Horizontal Spraying Inward.

3.1.1. Vertical Spraying Downward (VSD)

Figure 10 (a) presents the heat flux removed from the heated surface versus the difference between the heater surface temperature and the working fluid (R-134a) saturation temperature (DTsat) for the vertical spraying downward (VSD) orientation. The maximum heater power was limited by the DC power supply (500W) and restricted all tests from reaching critical heat flux (CHF), although it is expected to be very near 250 W/cm^2 . At low heat fluxes, under 100 W/cm^2 , the cooling performance (DTsat) demonstrated little dependence on acceleration in the vertical spraying downward orientation for this experiment. The data from the mid heat flux region, $100\text{-}200 \text{ W/cm}^2$, started to show a cooling separation between the 8g case and the 1.05-6g cases. The 8g cooling performance for this mid region operated approximately $0.5 \text{ }^\circ\text{C}$ cooler than the 1.05-6g test cases. The high heat flux region, $200\text{-}250 \text{ W/cm}^2$, shows a more evenly distributed cooling performance, maintaining the trend of increased performance with increased acceleration. This trend, at 250 W/cm^2 , spans nearly $3 \text{ }^\circ\text{C}$ between the 1.05g case and the 8g case, showing a clear performance improvement with increased acceleration near CHF.

Figure 10 (b) plots the acceleration resultant at the spray head versus the surface and saturation temperature difference, and shows many of the trends described in the above paragraph. For clarity, not all of the heat flux lines are shown. The plot shows “flat” regions (negligible changes in cooling performance) at the lower heat fluxes, whereas the high heat flux lines show an improving cooling performance (decreasing DTsat) with increasing acceleration.

This performance improvement could be explained by the improved fluid sweeping effect at high acceleration. The VSD orientation suggests that the acceleration vector is normal to the spray surface, when in fact it could be off up to 6° , as explained in Section 2.3. The orientation error is due to tubing/wiring attached to the rotating reservoir which restricts the reservoir’s alignment with the resultant acceleration vector. The VSD orientation error induces a “ramp” on the heater surface that allows fluid to be swept off of the heated surface due to acceleration. This additional force helps to remove “hot” fluid from the surface and replenish with “cold” fluid nearer to the surface which improves overall heat transfer.

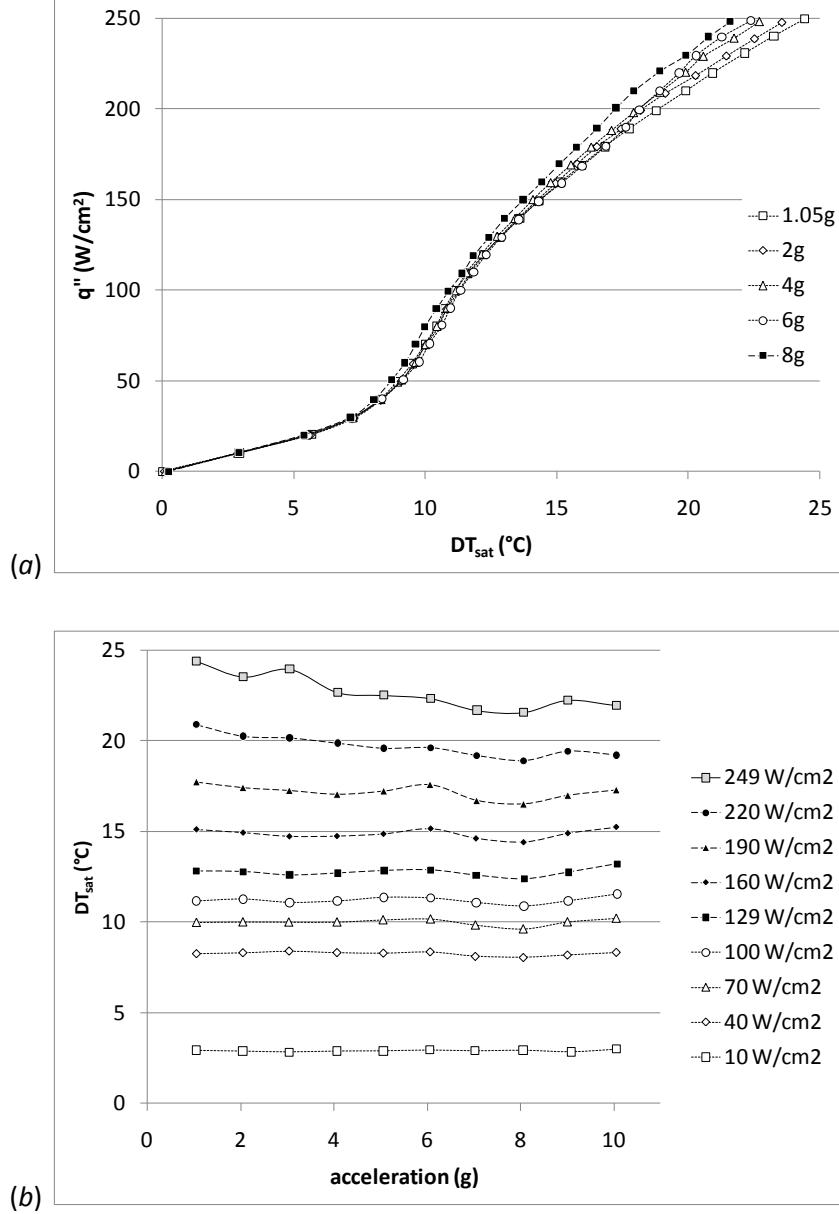


Figure 10: Steady State Cooling Performance For The Vertical Spraying Downward Orientation: (a) Heat Flux Vs. Surface Superheat; (b) Surface Superheat Vs. Acceleration ($T_{sat} = 22.66 \pm 2.33 \text{ } ^{\circ}\text{C}$, $DP = 11.59 \pm 0.83 \text{ psid}$).

3.1.2. Vertical Spraying Upward (VSU)

Figure 11s (a) & (b) illustrate the cooling performance variation associated with the vertical spraying upward (VSU) orientation. Figure 11 (a) shows this data on a heat flux versus surface superheat (ΔT_{sat}) plot. The overlapping data traces suggest very little change in performance due to acceleration. At approximately 60 W/cm^2 a small ($0.5 \text{ } ^{\circ}\text{C}$) improvement in the cooling performance begins and doesn't taper off until 140 W/cm^2 . This single-phase to two-phase transition region is the only region that demonstrates any appreciable difference in the cooling performance across all accelerations in the VSU orientation case.

Figure 11 (b) presents the data in a surface superheat versus acceleration plot, once again showing only a third of the heat flux lines to improve clarity. It can be seen that for the most part, all of the lines show a mostly horizontal trend, suggesting very little cooling performance dependence on acceleration. The only exceptions are the dips at the beginning of the 70, 99, and 129 W/cm² cases in the terrestrial acceleration tests as discussed in the above paragraph. Other “bumps” in the data lines, such as the 129, 159, and 188 W/cm² points in the 5g test case, are ignored because of the consistent nature of those “bumps” in the same acceleration test. Due to the way the tests were run, small discrepancies in the inlet/chamber pressure were typically carried through multiple heat flux levels (in the same acceleration test), but were always completely reset between differing acceleration runs.

The similarities in the data in the VSU tests are most likely an effect of the orientation. While gravity is acting against the spray, it is also acting with the fluid surface draining mechanisms. Due to the high momentum of the spray and the low residence time of the droplets between the spray nozzle and the heated surface (due to a very short path length), the droplet velocity does not decrease appreciably, although small momentum losses were expected. Additionally, when the fluid film is draining (falling off of the surface), an improved draining effect due to the increased body force would have suggested small gains due to decreasing film thickness. These expected small improvements may have been offset by the small declines in performance due to slight droplet momentum losses, therefore cancelling out any benefit or detriment.

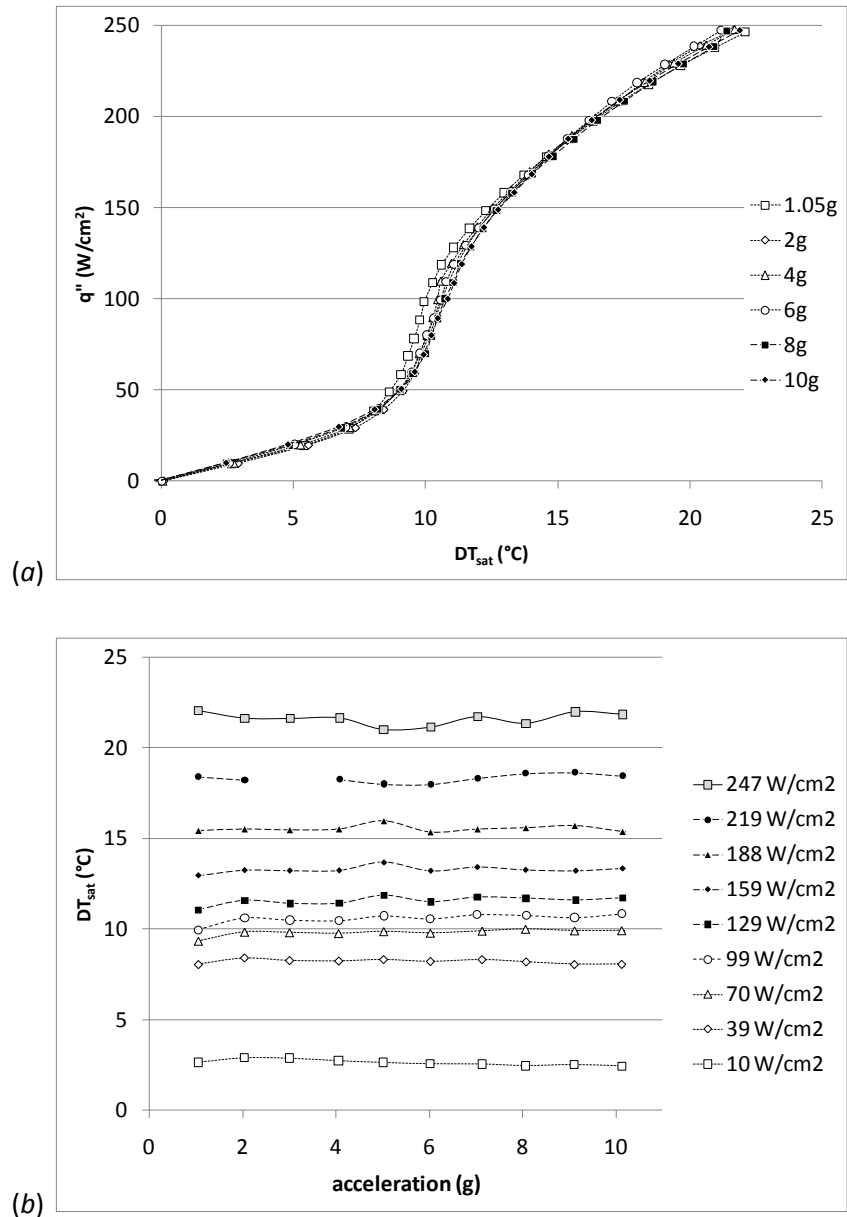


Figure 11: Steady State Cooling Performance For The Vertical Spraying Upward Orientation: (a) Heat Flux Vs. Surface Superheat; (b) Surface Superheat Vs. Acceleration ($T_{sat} = 23.82 \pm 2.85 \text{ }^{\circ}\text{C}$, $DP = 11.40 \pm 0.85 \text{ psid}$).

3.1.3. Horizontal Spraying Outward (HSO)

Figure 12 shows the data from the horizontal spraying outward (HSO) orientation tests. Figure 12 (a) presents the data on a heat flux versus surface superheat plot, while Figure 12 (b) plots the same data on a surface superheat versus acceleration graph. The first graph depicts the regularity in the results between accelerations, especially for heat fluxes below 189 W/cm^2 . Up to 189 W/cm^2 , all data traces overlap quite nicely; suggesting no cooling performance dependence on acceleration, for the HSO orientation. Above 189 W/cm^2 , a distribution between the 1.05g case and the 10g test begins to form. The cooling performance is the lowest (highest ΔT_{sat}) for the 1.05g case, but as the steady state acceleration improves, the cooling performance increases, all the way up through 10g's . Figure 12 (b) re-illustrates this point: the heat flux lines all maintain very comparable (horizontal lines) surface superheat values until the flux reaches 189 W/cm^2 , where a slight downward slope begins to form, suggesting improved performance with increased acceleration, up to 10g's .

Much like the VSD and VSU cases, the data from the HSO tests can be explained by orientation and body force effects. The HSO tests were oriented such that the spray was acting perpendicular to gravity and therefore the heated surface plane was parallel to centrifuge induced body force. An added sweeping effect (removal of fluid from the surface) would be expected at higher accelerations, but exhibited no appreciable performance gain below 189 W/cm^2 . This shift in cooling capability at high heat fluxes could be due to the added bubble activity on the surface which may allow the added body forces to help sweep away the fluid from bubble bursts, giving the incoming spray droplets the ability to penetrate further. At lower heat flux values, when the cooling is not completely dominated by latent heat transformation, the fluid would stay on the surface more easily (no bubbles bursting that would, like in the VSD orientation, return much of the fluid back to the surface due to orientation effects).

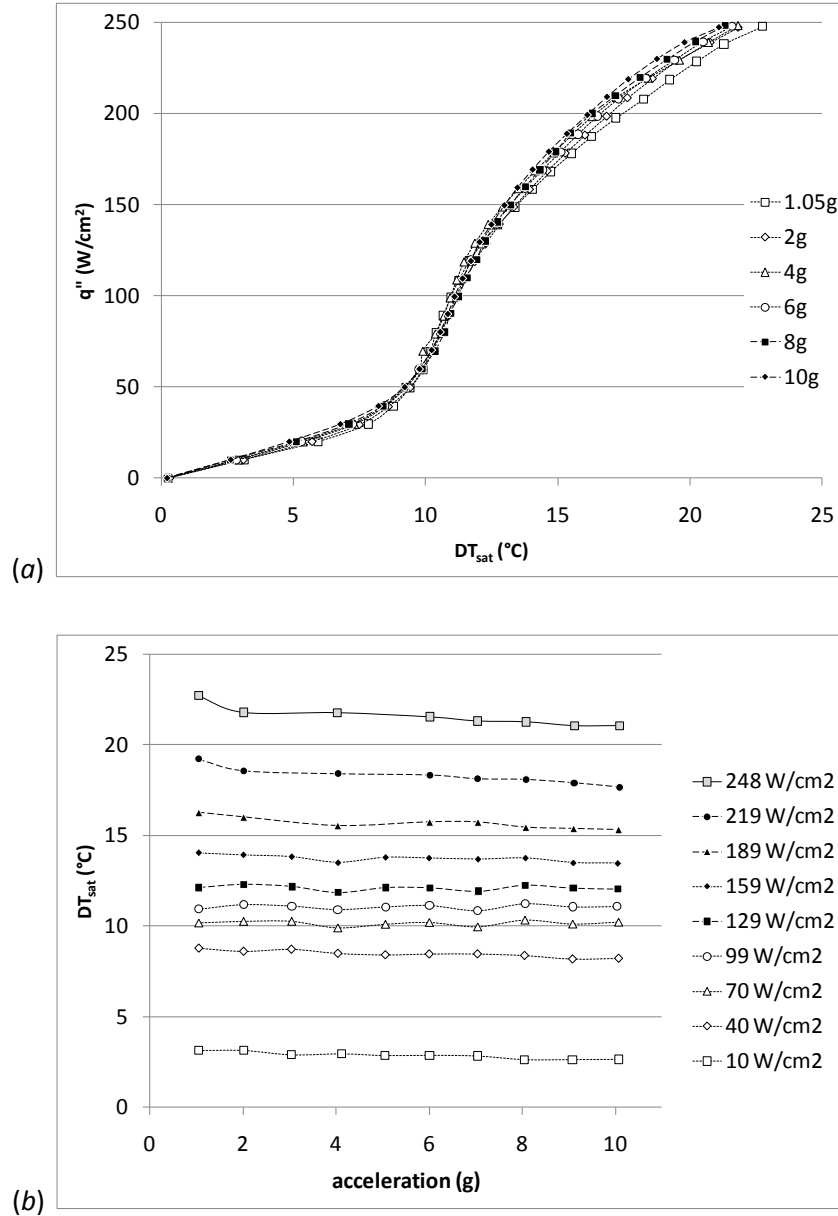


Figure 12: Steady State Cooling Performance For The Horizontal Spraying Outward Orientation: (a) Heat Flux Vs. Surface Superheat; (b) Surface Superheat Vs. Acceleration ($T_{\text{sat}} = 22.74 \pm 2.79 \text{ } ^\circ\text{C}$, $DP = 11.76 \pm 0.76 \text{ psid}$).

The last orientation tested was horizontal spraying inward (HSI). The HSI test results were expected to be very similar to the HSO tests due to the symmetry of the orientation. Additionally, during the HSI tests, errors were induced during data collection that compromised the accuracy of the data gathered. The results are shown in Appendix C, but due to the problems encountered during testing, no significant discussion is included.

3.2. Effect of Orientation

In addition to the comparisons of acceleration effect within each orientation, an evaluation was made at five acceleration set-points between the orientations. Figure 13-Figure 17 displays the effect of orientation for the following accelerations: 1.05g, 2g, 4g, 7g, and 10g.

In the 1.05g case, shown in Figure 13, a distinct cooling performance separation exists between all three orientations. The VSD is the worst performer, operating approximately 1-2 °C warmer than the HSO case for heat fluxes above 150 W/cm², while the VSU orientation operates from 1-2.5 °C cooler than the VSD case for fluxes ranging between 50-250 W/cm². This graph clearly shows the two-phase cooling performance improvement of the VSU and HSO cases over the nominal VSD case.

Additionally, the VSD orientation performs the worst in each of the plots, although the difference between the VSU and HSO test results becomes minimal above 2g.

The separation in performance between the VSD and VSU/HSO cases could be due to the film thickness effects which are a function of orientation. As mentioned previously, gravity in the VSD case propels the liquid toward the heated surface, which would increase the overall liquid film, enhancing the difficulty of “cool” spray droplets reaching the surface. In the VSU case, gravity effectively pulls excess liquid from the heated surface away from the film, making it thinner and therefore allowing the incoming droplets to penetrate closer to the surface and provide improved cooling. Similarly, gravity in the HSO case “sweeps” the surface of liquid, which again, allows the incoming spray droplets to penetrate the film and cool the heated surface more effectively.

As the acceleration increases, the cooling performance difference between the three orientations collapses slowly, until the 10g case. In Figure 17, which displays the three orientation tests at 10g's, some discrepancies to the previously mentioned trend are shown. Comparing the 7g case to the 10g case (Figure 16 & Figure 17), the cooling performance shift once again increases in the 130-200 W/cm² range to approximately 2 °C. The authors are uncertain as to the reason for this and assume uncertainty, experimental discrepancies, and competing physical phenomena to be the cause.

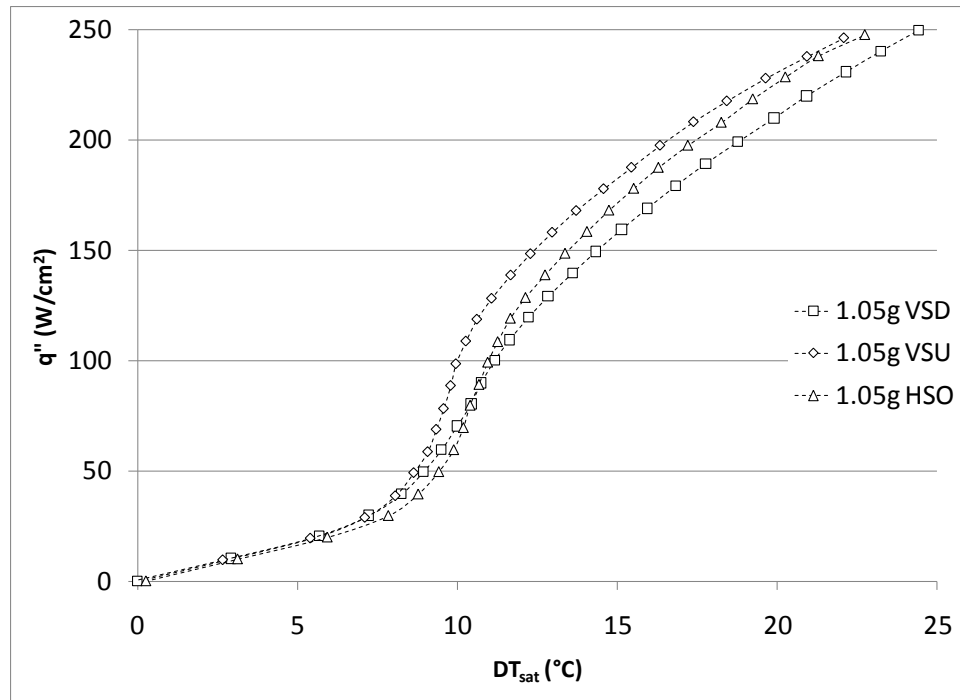


Figure 13: Steady State Cooling Performance For The 1.05g Case, Heat Flux Vs. Surface Superheat ($\alpha = 1.05 \pm 0.02$ g, $T_{sat} = 22.93 \pm 2.91$ °C, $DP = 11.63 \pm 0.66$ psid).

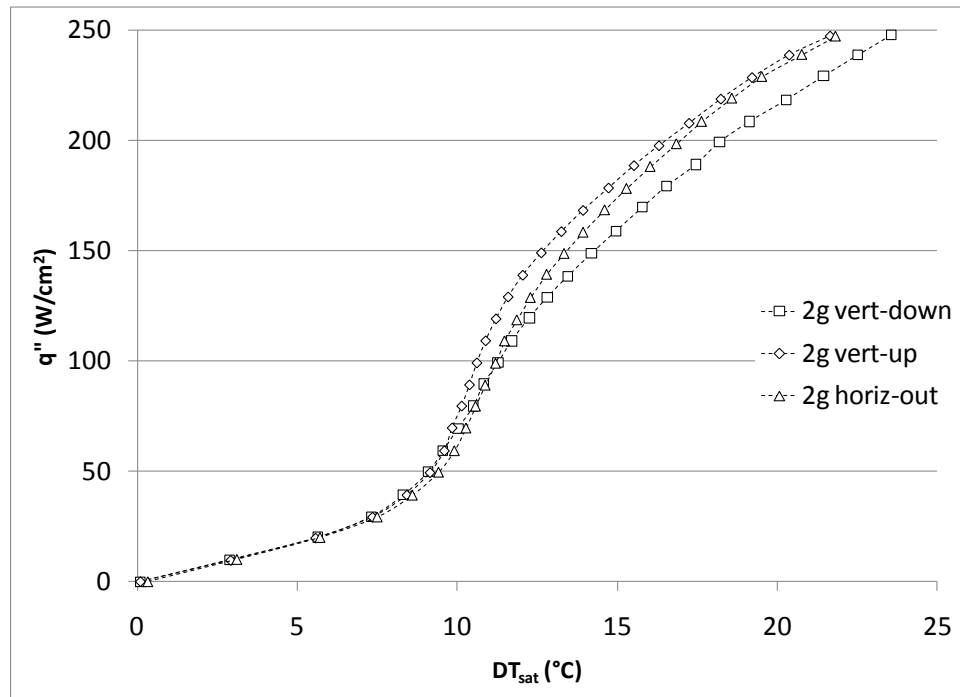


Figure 14: Steady State Cooling Performance For The 2g Case, Heat Flux Vs. Surface Superheat ($\alpha = 2.04 \pm 0.04$ g, $T_{sat} = 22.42 \pm 2.62$ °C, $DP = 11.53 \pm 0.62$ psid).

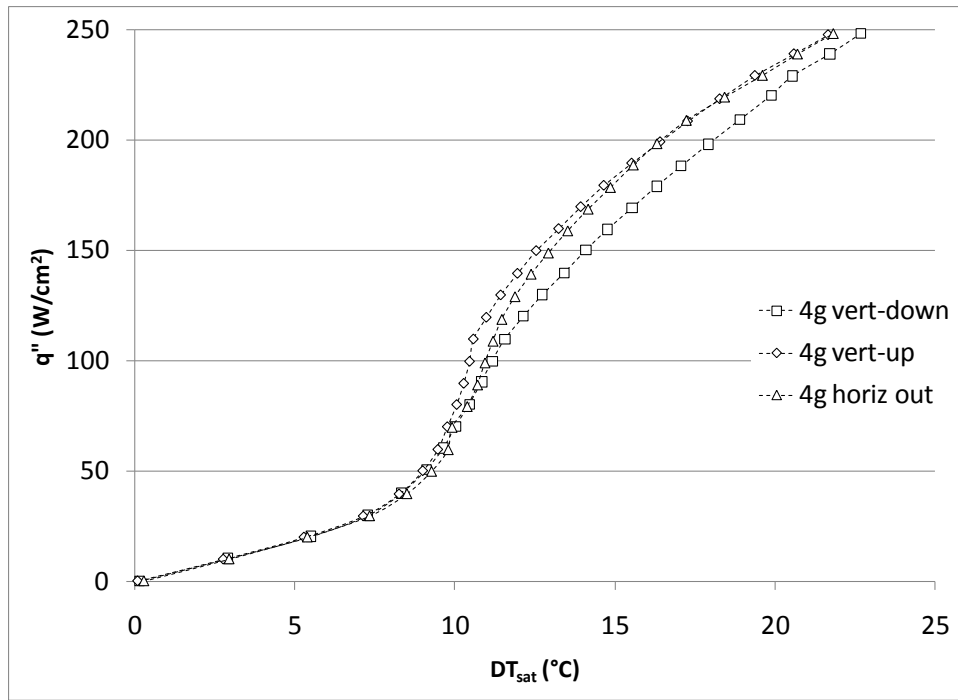


Figure 15: Steady State Cooling Performance For The 4g Case, Heat Flux Vs. Surface Superheat ($a = 4.06 \pm 0.04$ g, $T_{sat} = 23.16 \pm 3.11$ °C, $DP = 11.65 \pm 0.77$ psid).

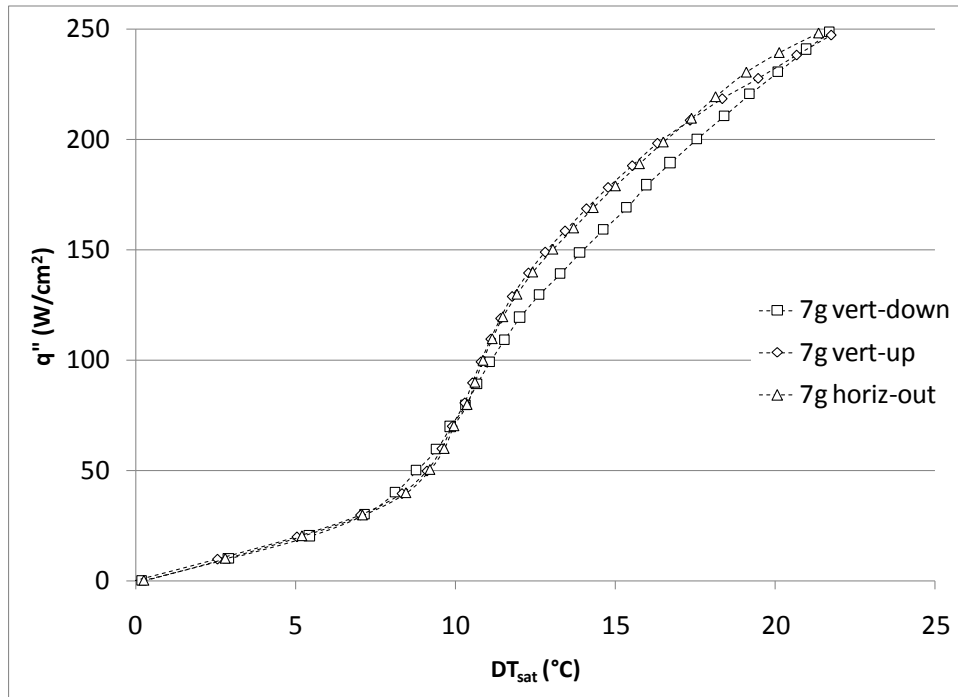


Figure 16: Steady State Cooling Performance For The 7g Case, Heat Flux Vs. Surface Superheat ($a = 7.06 \pm 0.06$ g, $T_{sat} = 22.99 \pm 2.55$ °C, $DP = 11.51 \pm 1.20$ psid).

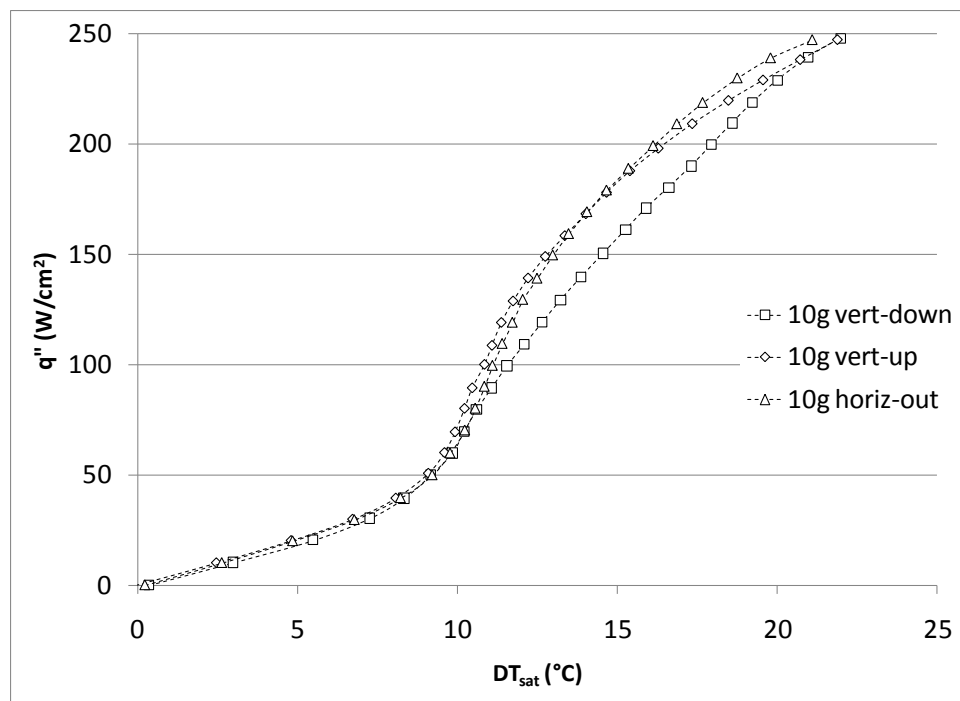


Figure 17: Steady State Cooling Performance For The 10g Case, Heat Flux Vs. Surface Superheat ($a = 10.09 \pm 0.06$ g, $T_{sat} = 23.51 \pm 2.70$ °C, $DP = 11.46 \pm 0.98$ psid).

4. Conclusions

The effects of elevated acceleration on the spray cooling performance of a two-nozzle array, using R-134a, were investigated under multiple orientations. The experimental apparatus, developed by RINI Technologies Inc., included a self-aligning spray-head that would swing-outward according to the table's rotational speed and a heated surface (relative direction dependent on the test's orientation). The effects of radial acceleration on each of three orientations were examined in addition to the effects of orientation at five constant accelerations were examined to determine trends in cooling performance.

In the vertical spraying downward (VSD) case, a performance improvement started to grow as acceleration increased at heat fluxes above 200 W/cm^2 . Although the data clearly shows a $3 \text{ }^\circ\text{C}$ difference between $1.05g$ and $10g$ at 250 W/cm^2 , this may have been an effect of the fluid sweeping off of the surface faster, resulting in a thinner liquid film formed on the heated surface.

The vertical spraying upward (VSU) case demonstrated consistent cooling performance through all accelerations; balanced cooling from combined effects. Spraying against gravity caused some droplet momentum loss that would have decreased performance, but gravity also reduced the fluid film thickness, causing a performance improvement. The conflicting factors provided a balancing effect that cancelled out any cooling performance improvement or deterioration.

During the horizontal spraying outward (HSO) tests, the cooling performance was improved at heat fluxes above 189 W/cm^2 with increasing acceleration. The fluid film sweeping effect was maximized for this case, exhibiting the largest effect in the most aggressive boiling regime.

The effect of orientation analysis compared the different orientations which have undergone the same acceleration (completed for $1.05g$, $2g$, $4g$, $7g$, and $10g$). A cooling performance enhancement was seen at $1.05g$ for the VSU and HSO cases over the VSD case. This enhancement was degraded as acceleration improved, demonstrating much less of an effect due to orientation at higher body forces.

5. Acknowledgements

The authors would like to thank the following individuals for their support: Jennifer Lindauer, Dave Courson, Andrew Fleming, and Marcus Sinewe. The authors would also like to thank RINI Technologies for their technical support of the hardware tested and University of Dayton Research Institute for their technician support in the experimental setup and testing phases.

6. Bibliography

Elston, L. J., K. L. Yerkes, S. K. Thomas, and J. McQuillen. "Cooling Performance of a 16-Nozzle Array in Variable Gravity." *Journal of Thermophysics and Heat Transfer*, 2009: Vol. 23, No. 3, Pgs 571-581.

Fleming, A. J. "The AFRL/RZPS Centrifuge Table Test Facility." *U.S. Air Force T&E Days*. Nashville, Tennessee, 2010.

Lin, L., and R. Ponnappan. "Two-Phase High Capacity Spray Cooling Loop: Nozzle Orientation Effects and Performance Results." *3rd AIAA International Energy Conversion Engineering Conference*. 2005.

Michalak, T. E., K. L. Yerkes, S. K. Thomas, and J. McQuillen. "Acceleration Effects on the Cooling Performance of a Partially Confined FC-72 Spray." *Journal of Thermophysics and Heat Transfer*, 2010: Vol. 24, No. 3, Pgs 463-479.

Selvam, R. P., M. T. Hamilton, J. E. Johnston, and E. A. Silk. "Thermal Modeling of Spray Cooling: Gravitational Effect on Droplet and Bubble Dynamics." *Journal of Thermophysics and Heat Transfer*, 2009: Vol. 23, No. 3, Pgs 560-570.

Silk, E. A., E. L. Golliher, and R. P. Selvam. "Spray cooling heat transfer: Technology overview and assessment of future challenges for micro-gravity application." *Energy Conversion and Management* 49, 2008: 453-468.

Yerkes, K. L., T. E. Michalak, K. M. Baysinger, R. Puterbaugh, S. Thomas, and J. McQuillen. "Variable-Gravity Effects on a Single-Phase Partially Confined Spray Cooling System." *Journal of Thermophysics and Heat Transfer*, 2006: Vol. 20, No. 3, Pgs 361-370.

Yoshida, K., Y. Abe, T. Oka, Y. Mori, and A. Nagashima. "Spray Cooling Under Reduced Gravity Condition." *Journal of Heat Transfer*, 2001: Vol. 123, No. 2, Pgs 309-318.

Appendix A

RINI Centrifuge Spray Cooling Experiment Standard Operation Procedure

The following is a step-by-step procedure to start and run the RINI Spray Cooling centrifuge experiment. Follow this procedure in exact order.

If any problems arise, make sure to hit the **Stop** button. Under only emergency circumstances should the **Abort** button be used to stop the system.

Procedure-

1. Turn on power to both TV's (linked to test-cell camera)
2. Switch power on to the centrifuge table
3. Switch power on to the RINI System
4. Turn on Mass Flow Control and Flow meter
5. Turn on the NESLAB HX-300 Chiller (Reach the pre-determined set point temperature)
6. Turn on both exhaust fans
7. Flip on breaker for "Centrifuge" power (Upstairs)
8. Turn on the power to the centrifuge motor
9. Close the outer test cell doors
10. Close the door to the adjacent test cell
11. Attach the safety sign to the outside test cell door
12. Flip on the active testing light beacon
13. Turn the power on to the Data Acquisition System and computer
14. Ensure the Centrifuge Controller is set on AUTO
15. Turn on the heater power supply
16. Start the LabView Program using the Run Button
17. A dialog box will appear asking if it is okay to save as _____ filename. Click ok
18. Hit the large "Record to File" button (Visible on the VI)
19. Enable the D/A Button (enables the heater, mass flow control, pump, and table spin speed)
20. Turn pump control on (adjust voltage so pressure drop is around 10 psi across the nozzle head)
21. Turn on the mass flow controller
22. Adjust mass flow controller to desired flow rate
23. Turn table control on
24. Adjust the table to the desired acceleration
25. Turn heater on
26. Adjust the heater (according to test plans)

Appendix B

RINI Centrifuge Spray Cooling Experiment Standard Shutdown Procedure

The following is a step-by-step procedure to finish running and shut down the RINI Spray Cooling Centrifuge experiment. Follow this procedure in exact order.

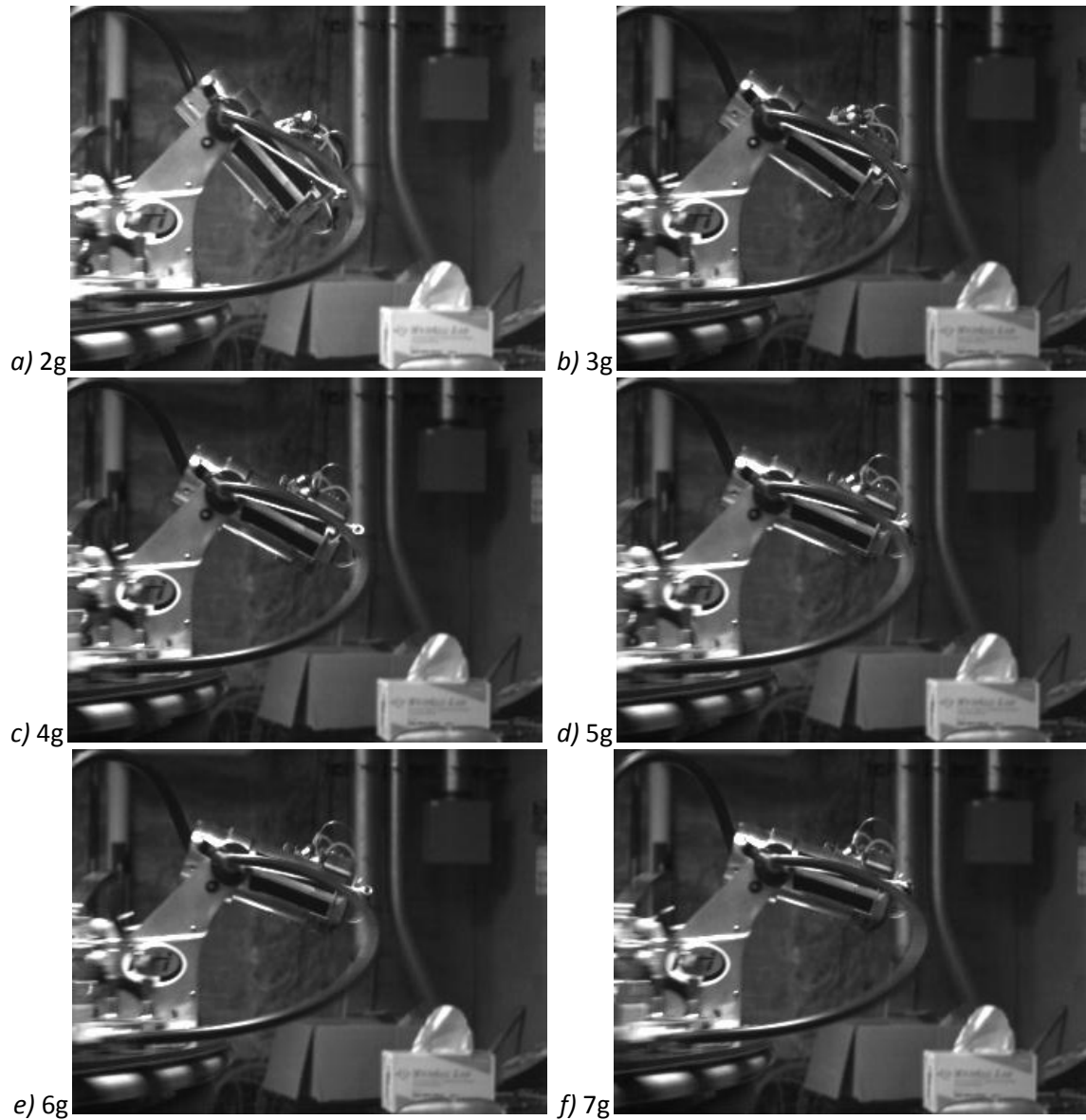
If any problems arise, make sure to hit the **Stop** button. Under only emergency circumstances should the **Abort** button be used to stop the system.

Procedure-

1. Ramp down the heater
2. Turn the heater off
3. Ramp down the table
4. Turn the table control off
5. Open the mass flow controller valve
6. Turn off the mass flow controller
7. Turn pump control off
8. Disable the D/A Button
9. Turn off the heater power supply
10. Flip off the active testing light beacon
11. Take off the safety sign from the outside test cell door
12. Open the outer test cell doors
13. Turn off power to the centrifuge motor
14. Turn off the exhaust fans
15. Flip off the breaker for the “Centrifuge” power (upstairs)
16. Turn off the NESLAB HX-300 Chiller
17. Turn off the Mass Flow Controller and Flow meter
18. Switch off the power to the RINI System
19. Switch off the power to the centrifuge table
20. Turn off the power to both TV's

Appendix C

Acceleration vector alignment error



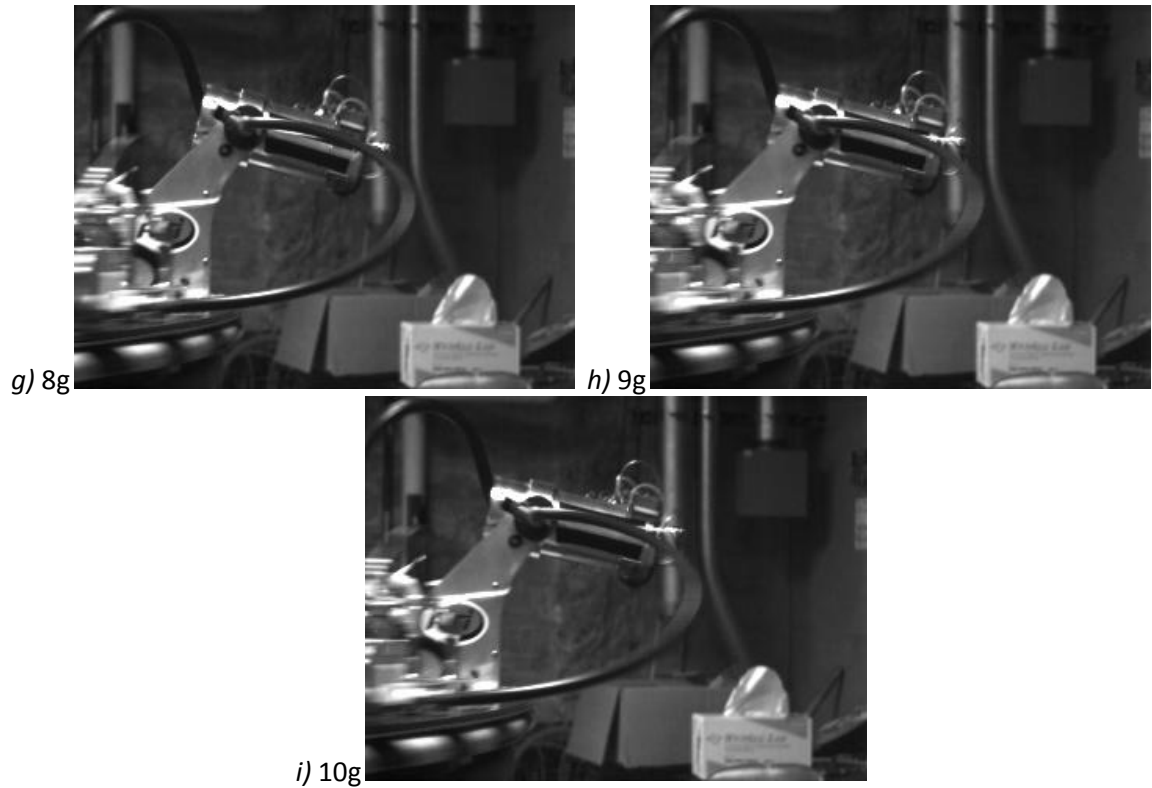


Figure C-1: Acceleration Vector Alignment Error For 2g-10g Cases: (a) $2g=5.5^\circ$; (b) $3g=7.0^\circ$; (c) $4g=6.5^\circ$; (d) $5g=9.5^\circ$; (e) $6g=7.4^\circ$; (f) $7g=8.3^\circ$; (g) $8g=13.7^\circ$; (h) $9g=6.6^\circ$; (i) $10g=5.8^\circ$.

Appendix D

Horizontal Spraying Inward (HSI)

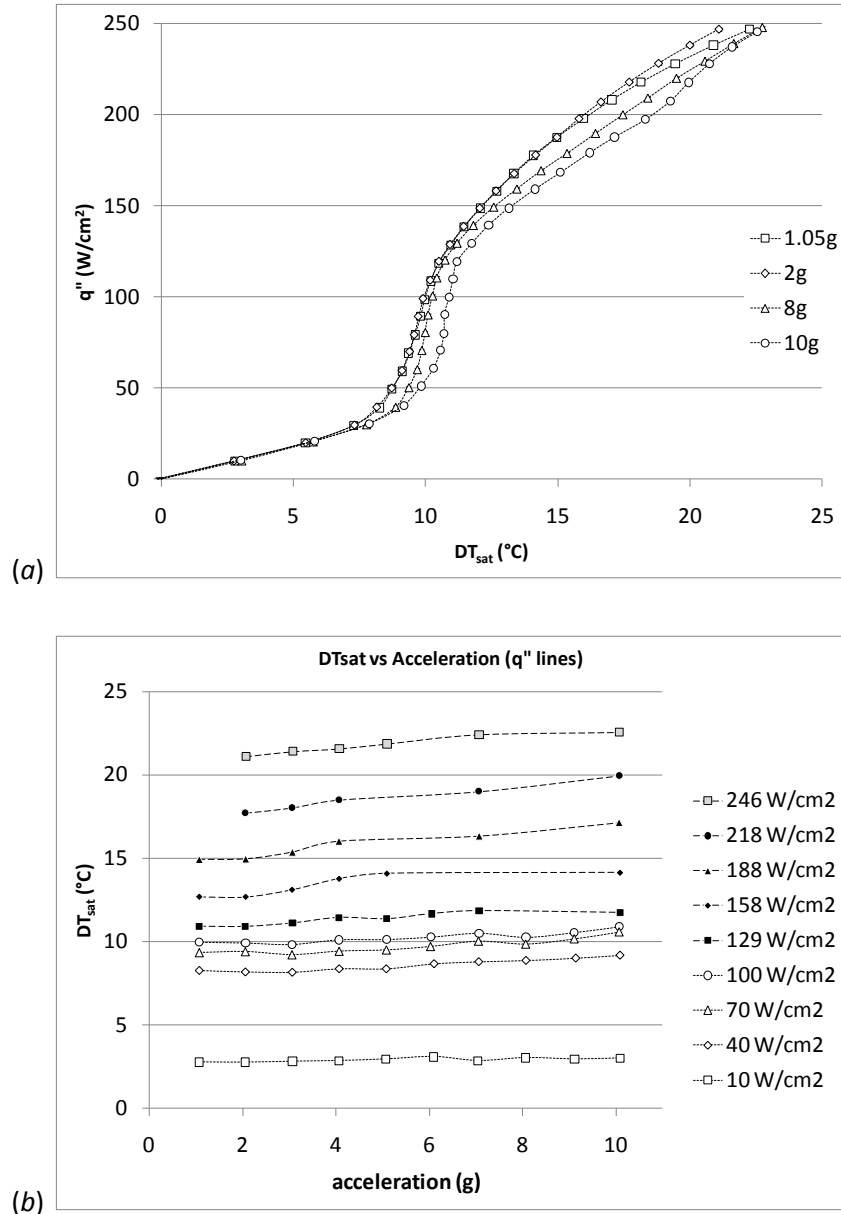


Figure D-1: Steady State Cooling Performance For The Horizontal Spraying Inward Orientation: (a) Heat Flux Vs. Surface Superheat; (b) Surface Superheat Vs. Acceleration ($T_{sat} = 23.24 \pm 3.46$ °C, $DP = 11.50 \pm 0.96$ psid).

Appendix E

Acceleration Calculation of the Heated Surface during Centrifuge Testing

Below are the equations, defined properties, and methods we used to find the acceleration of the heater. The measurements we converted to the metric system to be used in the equations. The labview vi uses a slightly different nomenclature for the acceleration on the surface of the heater: a_{spray} instead of a_{heater} .

Definitions-

ω = Rotational Speed of the Table

r = Radius to the Object of Interest (from center of the table)

a = Acceleration of the Object

i = Initial (when added to the end of the name of an object on the table)

Defined Properties-

$r_{accelerometer} = 1.2192 \text{ m (48 inches)}$

$r_{heateri} = 1.2129 \text{ m (47.75 inches)}$

$r_{resistor} = 0.15875 \text{ m (6.25 inches)}$

Equations-

$$a_{heater} = \omega^2 * r_{heater}$$

$$r_{heater} = r_{heateri} + (r_{resistor} * \cos \theta)$$

$$\theta = \tan^{-1}\left(\frac{a_{accelerometer}}{1}\right)$$

$$\omega = \sqrt{\frac{a_{accelerometer}}{r_{accelerometer}}}$$

Work to Find the Acceleration of the Heater-

To find the overall acceleration of the heater, two terms need to be defined and be plugged into the first equation, $a_{heater} = \omega^2 * r_{heater}$. The terms are ω and r_{heater} . These two were found in the following order.

$$\omega = \sqrt{\frac{a_{accelerometer}}{r_{accelerometer}}} = \sqrt{\frac{a_{accelerometer}}{1.2192 \text{ m}}}$$

$$r_{heater} = r_{heateri} + (r_{resistor} * \cos \theta) = 1.2129 \text{ m} + (0.15875 \text{ m} * \cos \theta)$$

$$\theta = \tan^{-1}\left(\frac{1}{a_{accelerometer}}\right)$$

$$a_{heater} = \omega^2 * r_{heater} = \frac{a_{accelerometer}}{1.2192 \text{ m}} * [1.2129 \text{ m} + (0.15875 \text{ m} * \cos(\tan^{-1}(\frac{1}{a_{accelerometer}})))]$$

Appendix F

Structural Analysis



582 South Econ Circle • Oviedo, FL 32765 • 407/359.7138 • www.rinitech.com

RTI Centrifuge System Structural Analysis December 22, 2006

Table of Contents

1. System Overview	1
2. Reservoir Strut Analysis.....	2
3. Screw Shearing Analysis	4
4. Screw Tensile Analysis	6

1. System Overview

The RTI centrifuge system consists of a two nozzle array mounted on a tilting refrigerant reservoir, an RTI Wankel pump, a plate heat exchanger, and flexible refrigerant hoses. These are all bolted to a quarter inch thick aluminum base plate, which in turn is bolted to the centrifuge table. The pump is made of aluminum and steel parts, the heat exchanger is copper brazed steel plates, and the reservoir is mostly aluminum. All fittings are brass. The reservoir is assembled with 18-8 stainless steel screws.

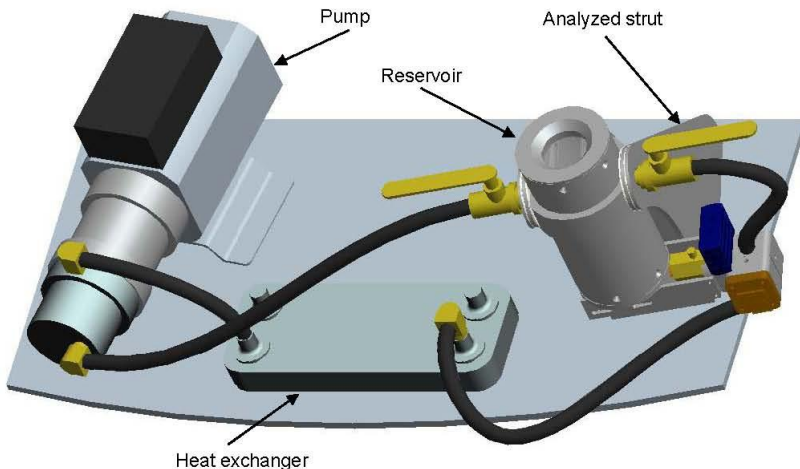


Figure 1. RTI centrifuge system components



2. Reservoir Strut Analysis

The reservoir has a mass of approximately 2 kg including hardware and other components attached to it and these are supported by two struts like the one shown in Figure 2. The analysis below was done for 100 m/s^2 which is slightly greater than ten G forces. At this acceleration the 2 kg weighs 40.1 lbf. Since there are two struts, one strut bears approximately 20 lbf. This force was spread uniformly over the cross-sectional area of the inside bearing surface of the strut in the direction it would be at 10 G forces. The analysis in Figure 3 shows that the maximum stress experienced is 1396 lbf/in^2 . The tensile yield strength for 6061 aluminum is 40000 lbf/in^2 ^a, so there is a safety factor of 28 for the strut.

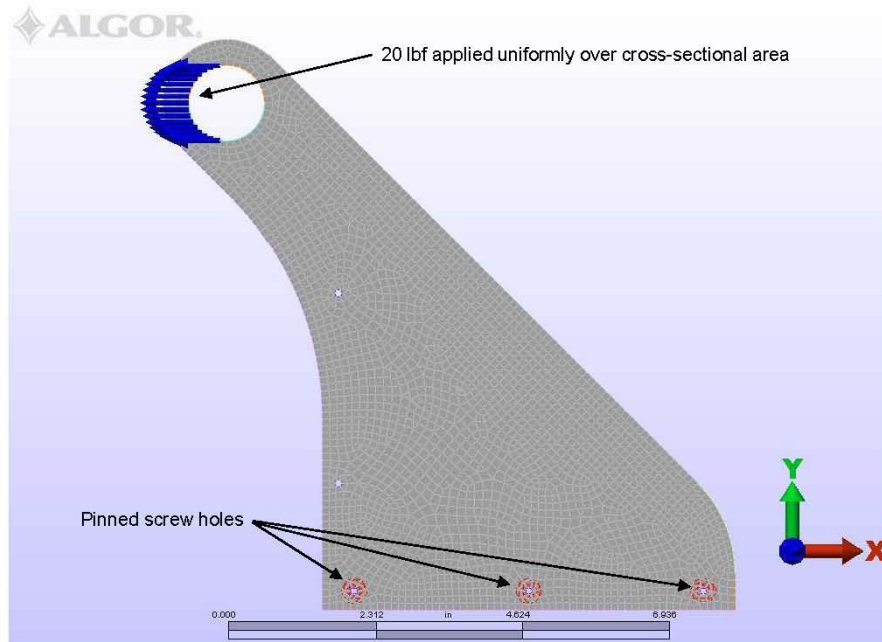


Figure 2. Constraints and forces on strut

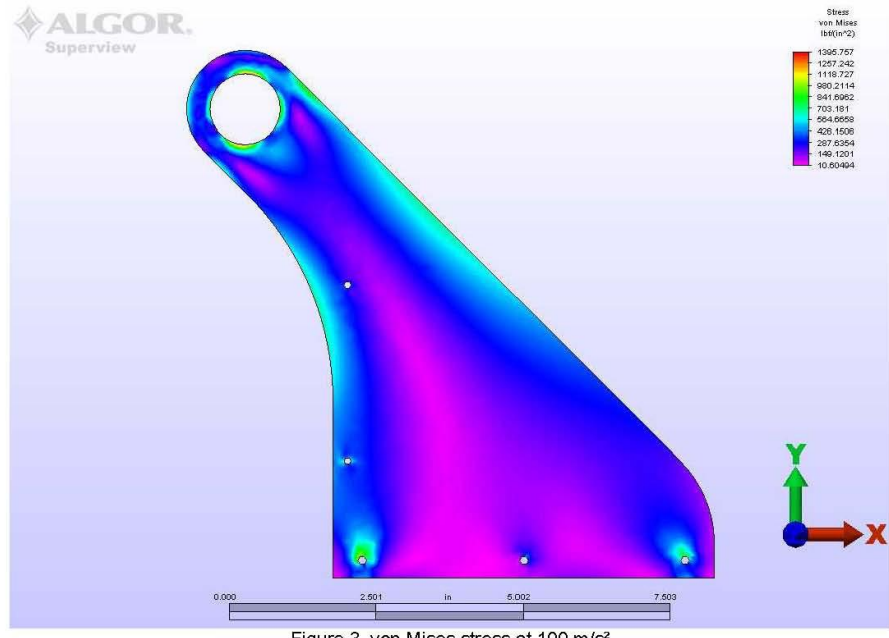


Figure 3. von Mises stress at 100 m/s²

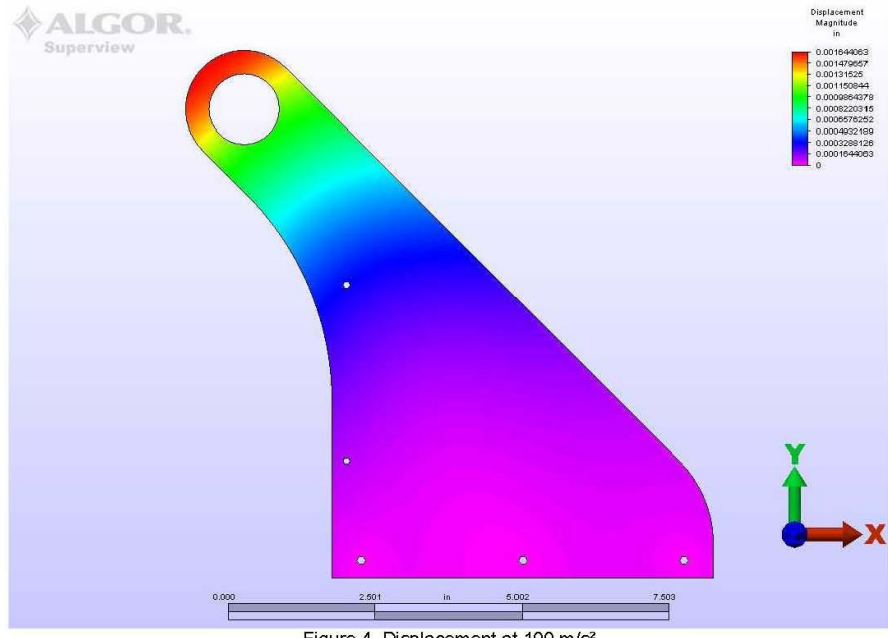


Figure 4. Displacement at 100 m/s^2

3. Screw Shearing Analysis

Table 1 summarizes the analysis done on bolts that will fasten components to the base plate and the total assembly to the centrifuge table as shown in Figure 5. The shear stress is calculated using the relations in Equation 1. The tensile yield strength of the 18-8 (Type 304) stainless steel screws is 31200 psi^b and the shear strength is approximately 0.6^c times the tensile strength so shear yield strength is 18720 psi. Thus the smallest shear yield safety factor is 11.

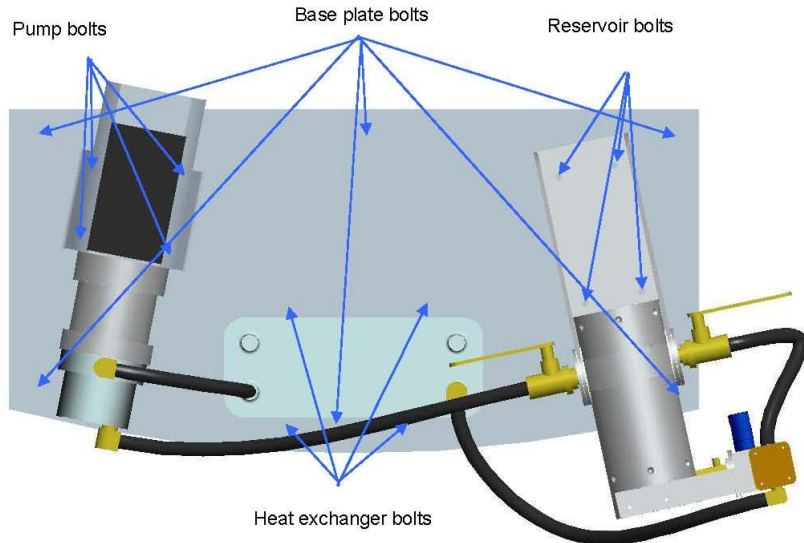


Figure 5. Locations of analyzed bolts under shear stress

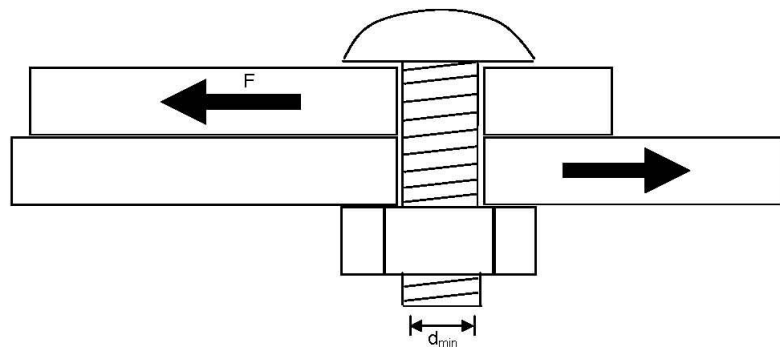


Figure 6. Shear stress on bolts

$$\tau = \frac{F}{A} \quad A = \frac{\pi \cdot d^2}{4}$$

Equation 1. Finding shear stress on a screw

Table 1. Analysis of shear stress on screws

	Mass (kg)	Force @ 100 m/s ² (N)	Force (lbf)	# of screws	Force/screw (lbf)	Screw size	Screw area (in ²)	Shear stress (psi)
HX	1.5	150	34	4	8.5	1/4 - 20	0.0318	267
Pump	5.6	560	126	4	31.5	10 - 32	0.02	1575
Reservoir	2.8	280	63	4	15.8	1/4 - 20	0.0318	495
Base plate	3.2	320	72					
Hoses & fittings	1.2	120	27					
Total	14.3	1430	322	6	53.7	1/4 - 20	0.0318	1688

4. Screw Tensile Analysis

Table 2 summarizes the analysis done on the bolts with the greatest tensile stresses. Figure 7,Figure 8,Figure 9 show how the moments are balanced to find the tensile force on the screws. The tensile yield strength of the 18-8 (Type 304) stainless steel screws is 31200 psi so the smallest tensile yield safety factor is 14.

All bolts in these calculations, except for the pump bolts, will be used with nuts of the same material to avoid the possibility of stripping threads tapped into aluminum. The pump has holes tapped into 0.1 inches of aluminum on its housing. The aluminum thread shear area is 0.0234 in² and at 85 lbf per tapped hole the threads experience 3630 psi of shear stress. The tensile yield strength for 6061 aluminum is 40000 psi thus the shear yield strength is 24000 psi (40000*0.6) and the safety factor for the tapped holes is 6.

Table 2. Tensile stress on bolts

	Mass (kg)	Force @ 100 m/s ² (N)	Force (lbf)	Tensile force on screws (lbf)	# of back screws	Force/screw (lbf)	Screw size	Screw area (in ²)	Tensile stress (psi)
Reservoir	2.8	280	63	92	2	46	1/4 - 20	0.0318	1447
Pump	5.6	560	126	85	2	43	10 - 32	0.02	2125
Total	14.3	1430	322	113	3	38	1/4 - 20	0.0318	1184

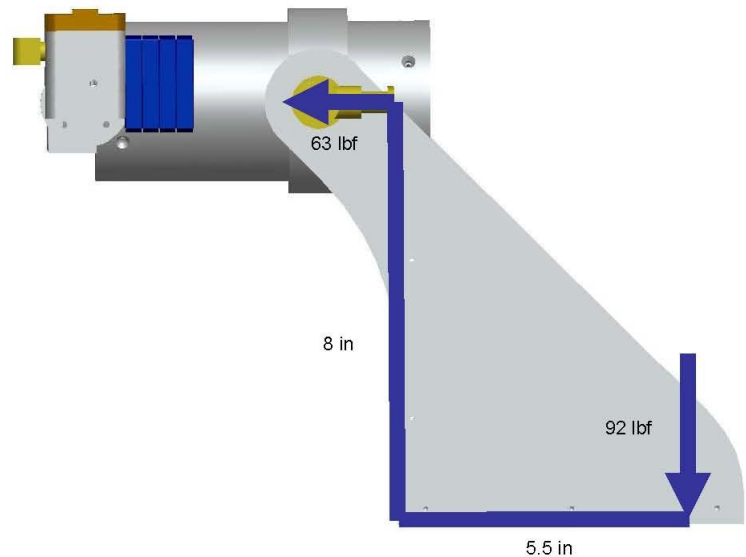


Figure 7. Tensile force on reservoir bolts

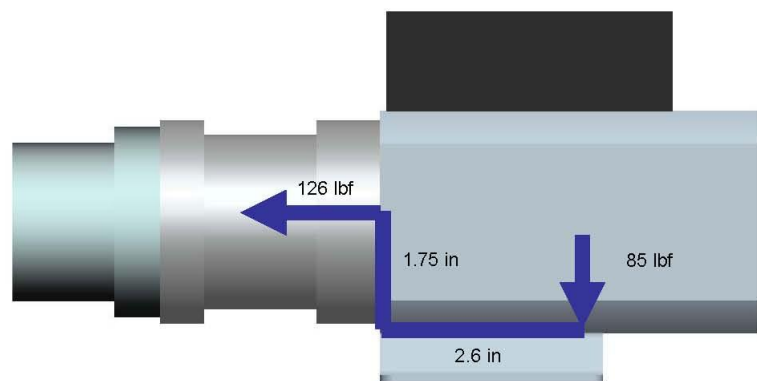


Figure 8. Tensile force on pump screws

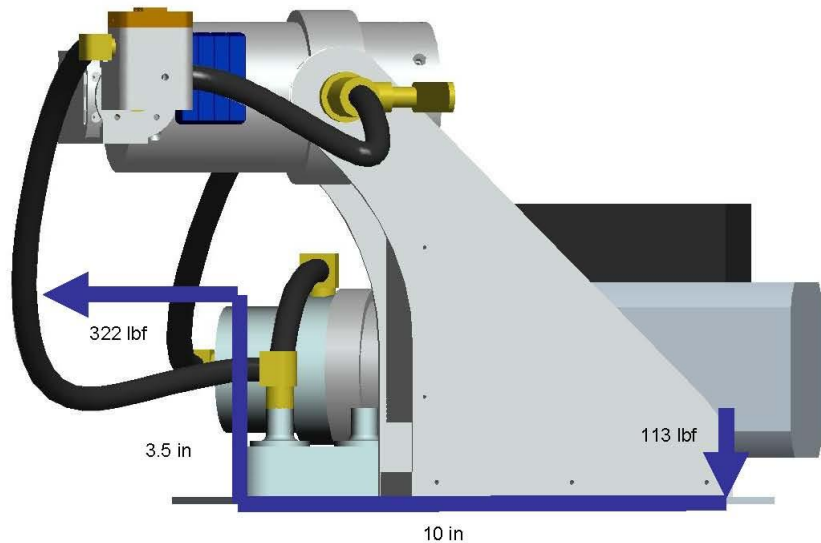


Figure 9. Tensile forces on base plate bolts

- ^a <http://www.matweb.com/search/SpecificMaterial.asp?baseNum=MA6061T6>
- ^b <http://www.matweb.com/search/SpecificMaterial.asp?baseNum=MQ304A>
- ^c <http://www.boltscience.com/pages/faq.htm>
- ^d http://www.roymech.co.uk/Useful_Tables/Screws/Thread_Calcs.html

Appendix G

Test Plan

RINI Centrifuge Spray Cooling

21 December 2009

**AFRL/RZP Energy/Power/Thermal Division
1950 Fifth St.
Wright-Patterson AFB, OH 45433-7251**

Prepared By:

**Levi J. Elston
AFRL/RZPS**

DESTRUCTION NOTICE – For unclassified, limited documents, destroy by any method that will prevent disclosure of contents or reconstruction of the document.



**AIR FORCE RESEARCH LABORATORY
Propulsion Directorate
1950 Fifth St.
AIR FORCE MATERIEL COMMAND
WRIGHT-PATTERSON AIR FORCE BASE, OH 45433-7251**

EXECUTIVE SUMMARY

Test Objective: To evaluate RINI spray cooling (2-nozzle) system operation under high-g loading.

Background: The test system was created/assembled under contract # FA8650-06-D-2620 DO-0002. As part of that contract, AFRL agreed to centrifuge testing (steady state only) of the system.

Test Item Description: The RINI centrifuge evaporative spray cooling system consists of a 2-phase pump, reservoir, nozzle head (with heater), and condenser. The working fluid is R-134a and operates from 10-60 °C. The nozzle head consists of 2 spray-nozzles (vapor atomization) cooling a heated area of 2 cm². The condenser is cooled via an off-table chiller (working fluid = 100% ethylene glycol).

Test Methodology: The tests will be conducted remotely (control room #2) for safety reasons. All of the control and data acquisition for the tests will be done from a computer console. The appended standard operating procedure provides details of startup of all of the necessary systems (chiller, centrifuge, data acquisition/control, etc.). Next the acceleration is set to a specific acceleration (e.g. 5 g's), the spray pump is dialed into a desired nozzle pressure drop (e.g. 11 psid), and the chiller flow rate is set via a combination of a remote controlled mass flow controller and/or a remote controlled booster pump (e.g. 0.5 gpm). The data is collected via an Agilent data acquisition system with LabView operation/control (cycle time is approximately 1.6 Hz).

Technical Risk: The largest contributor to risk is the uncertainty due to signal fluctuation (table slip rings). Other potential contributors to technical risk are: accuracy of nozzle head swingout (correct angle associated resultant acceleration), ambient convection effects (spinning in air at high speed), and limitations in control (e.g. chiller flow rate).

Safety: The only major safety risk is that associated with the spinning table. The SOP has been generated to reduce this overall risk considerably (closed door, warning beacon, etc.)

Environmental Impact: During fill/evacuation of refrigerant (R-134a is working fluid), some will be lost to the environment. The quantity is expected to be very small (~0.1 lb) and will have very little environmental impact because R-134a is non-ozone depleting.

This test plan was prepared by the AFRL/RZPS thermal group.

Date:

Levi J. Elston
Author, AFRL/RZPS

This test plan has undergone a technical review and is complete:

Larry Byrd
AFRL/RZPS

Technical Risk is: _____ Date:

(low/med/high)

Approved/Disapproved

Andrew Fleming
Work Unit Manager

Date:

G1.0 INTRODUCTION

G1.1 GENERAL

The purpose of the testing is to generate high-g steady state testing of an evaporative spray cooling system. Additionally, the testing has already been funded through the above mentioned Congressional Interest Item. The testing will evaluate cooling performance as a function of acceleration (1-10 g's) and nozzle orientation (with respect to the acceleration vector). The metrics for successful test include: acquiring accurate and stable data to build performance graphs (ΔT_{sat} vs. q'') as a function of the acceleration vector and nozzle orientation. The test plan is expected to take approximately 1 month to execute.

G1.2 BACKGROUND

The system was delivered in July 2007. It was installed on the table at that time, but never reached the testing stage and was removed from the table in August 2007. The system was put into storage for approximately 2 years when it was reinstalled on the table in May-June 2009. The long-term storage of the system allowed for corrosion of parts which added significant time/effort when reinstalled 2 years later.

G2.0 TEST OBJECTIVES AND MEASURES

The following critical issues and objectives and corresponding measures will be evaluated during this test. The test objectives are derived from the critical issue statement.

The primary objective of this test is to determine the effect of body forces (and body force orientation) on the cooling performance of a 2-nozzle (with a 2 cm^2 heated surface) evaporative spray cooling (ESC) system. To properly measure this objective, the tests will control and acquire the following data:

Control: table spin speed (acceleration), refrigerant flow rate (nozzle pressure drop), heater power (heat removed by ESC), and chiller flow rate (to maintain a stable saturation temperature).

Acquire: 4 temperatures in heater block (between heater and spray surface), saturation temperature in spray chamber, condenser temperature (chiller side), nozzle pressure, chamber pressure, acceleration, heater voltage, heater current.

A baseline for comparison was done before delivery of the system in 2007 (completed at contractor's facilities). This will be used to compare the 1-g data to check for accuracy and hardware issues.

The test will be operated by first setting a nozzle orientation, then acceleration, a desired saturation temperature, and nozzle pressure drop. During a test, the orientation and acceleration will remain constant while the heat input to the system is systematically adjusted (0-500 W in 20 W increments). During the test, the saturation temperature will be held constant via controlling the chiller flow rate controls (mass flow controller and booster pump). After the system reaches a steady-state at a given data point, approximately 100 data points will be recorded for further data reduction (1 data point is hand recorded at each steady state portion, sample hand recording sheet is appended). Each of these tests will generate a performance curve at a given acceleration and nozzle orientation which will be compared upon conclusion of the testing.

G3.0 TEST ITEM DESCRIPTION (may be n/a if this is not an item test)

A detailed description of the test item is appended that includes: design, baseline (1-g) performance testing, a preliminary test plan, high-g stress analysis, and a R-134a safety evaluation.

G4.0 TEST LOCATION

The centrifuge table facility in Building 71B, H-bay is required for the testing.

G5.0 TEST SCHEDULE

The proposed schedule for testing is highlighted in Table G-1 (table shows experimental setup time, testing time, and data reduction/reporting time).

Table G-1 RINI Centrifuge Evaporative Spray Cooling Schedule.

	4-May	11-May	18-May	25-May	1-Jun	8-Jun	15-Jun	22-Jun	29-Jun	6-Jul	13-Jul	20-Jul	27-Jul	3-Aug	10-Aug	17-Aug	24-Aug	31-Aug	7-Sep	14-Sep	21-Sep	28-Sep	
Install on table	X	X	X	X																			
Data acquisition connection		X	X	X	X																		
Combine VI's (RINI's & Flem's)					X	X	X	X	X	X	X	X	X	X	X	X	X	X					
Calibration (TC, Press)										X	X	X	X									X	
Rebalance table																							
Maintenance/Re-tightening					X	X	X							X	X	X	X						
Leak Check/Fix										X	X	X	X	X	X	X	X	X	X	X	X	X	
New Plumbing														X	X								
Motor Controller																							
Baselines																							
Vertical Spraying Up 1-10g																							
Vertical Spraying Down 1-10g																							
Horizontal Outward 1-10g																							
Horizontal Inward 1-10g																							
Data Reduction																							
Tech Report																							
Program Management	X	X	X	X	X	X	X	X	X	X	X	X	X	X	X	X	X	X	X	X	X	X	X

	5-Oct	23-Nov	30-Nov	7-Dec	14-Dec	21-Dec	28-Dec	4-Jan	11-Jan	18-Jan	25-Jan	1-Feb	8-Feb	15-Feb	22-Feb	1-Mar	8-Mar	15-Mar	22-Mar	29-Mar		
Install on table																						
Data acquisition connection																						
Combine VI's (RINI's & Flem's)																						
Calibration (TC, Press)																						
Rebalance table																						
Maintenance/Re-tightening																						
Leak Check/Fix																						
New Plumbing																						
Motor Controller																						
Baselines																						
Vertical Spraying Up 1-10g																						
Vertical Spraying Down 1-10g																						
Horizontal Outward 1-10g																						
Horizontal Inward 1-10g																						
Data Reduction																						
Tech Report																						
Program Management																						

G6.0 CONSTRAINTS AND LIMITATIONS

The only expected constraints to the proposed test schedule would be unforeseen delays (such as finding/fixing leaks; already lost >1 month) and testing time duration which is expected to be approximately 1 month, but that could slip a couple of weeks either way.

Other constraints associated with data collection accuracy are related to inherent oscillations with slip ring signal transfer.

G7.0 TEST RESOURCES

G7.1 FACILITIES / TEST RANGE

N/A

G7.2 SUPPORT REQUIREMENTS

The testing requires the support of a technical approving authority, a safety approving authority, and all equipment associated with the centrifuge testing facility (e.g. restricted access to test cell #4 and undeniable use of the control system for the centrifuge facility-in control room 2).

G8.0 INSTRUMENTATION

All instrumentation is monitored and recorded via the data acquisition system in control room 2. The instruments used, quantity, type, range, and accuracy is shown in Table G-2. Each of these measurements are sampled at approximately 1.6 Hz. The remote control aspect is made via the controls described in Table 3 shows the control devices used and their control ranges. The steady state acceleration was controlled via the electrical motor speed controller that was operated in the centrifuge control room. The nozzle pressure drop, with a design point of 10-12 psid, was controlled by the variable speed pump controller output from the data acquisition system (signal transferred through slip rings to “on-table” controller). Similarly, the flow rate was controlled with the data acquisition system output control. Additionally, for higher flow rate, the booster pump speed was adjusted using the pump speed controller mounted inside the centrifuge table control room. Lastly, the heater power was adjusted using a low voltage signal from the data acquisition system to control the output power of the “off-table” heater power supply.

Table G-2 Instrument quantity, type, range, and accuracy.

Measurement	Sensor Type	Range	Accuracy
Thermocouples (6)	Thermocouples (Type T)	Calibrated (0-100 °C)	±0.62 °C
Pressure (2)	Pressure Transducers	Calibrated (0-100 psig)	±0.14 psig
Flow meter (1)	Piston	0-5 gpm	±
Heater power (2)	Voltmeters (w/ precision resistor for current measurement)	0-500 W	±
Acceleration (1)	3-axis accelerometer	0-10 g	±
Accuracy assumes noiseless data (slip rings will increase these values)			

Table G-3 Control devices.

Control	Controller Type	Control Range	Response Range
Acceleration	Potentiometer Motor Controller	0-10 V	0-10 g's
Nozzle Pressure Drop (Pump Speed)	Computer D-A Output	0-5 V	0-15 psid
Ethylene Glycol Flow Rate (Chiller)	MFC-Computer D-A Output Booster Pump-Potentiometer Motor Controller	4-20 mA 0-40%	0-1 gpm
Heater Power	Computer D-A Output	0-5.25 V	0-500 W

G9.0 PRE-TEST PREDICTIONS

All pre-test predictions come from contractor provided baselines a 1-g.

G10.0 DATA HANDLING REQUIREMENTS

The display during testing is shown in Figure G-1, Figure G-2, and Figure G-3. The LabView Front Panel is split up over 3 screens. The first screen (Figure G-1) is dedicated solely to control with some feedback associated with these controls. The second screen (Figure G-2) shows 4 strip charts that are used for indication as well as steady state determination. The third and final screen (Figure G-3) displays the simplistic flow loops, specific thermocouple and pressure data, and a chart that lists the data for hand recording during the testing.

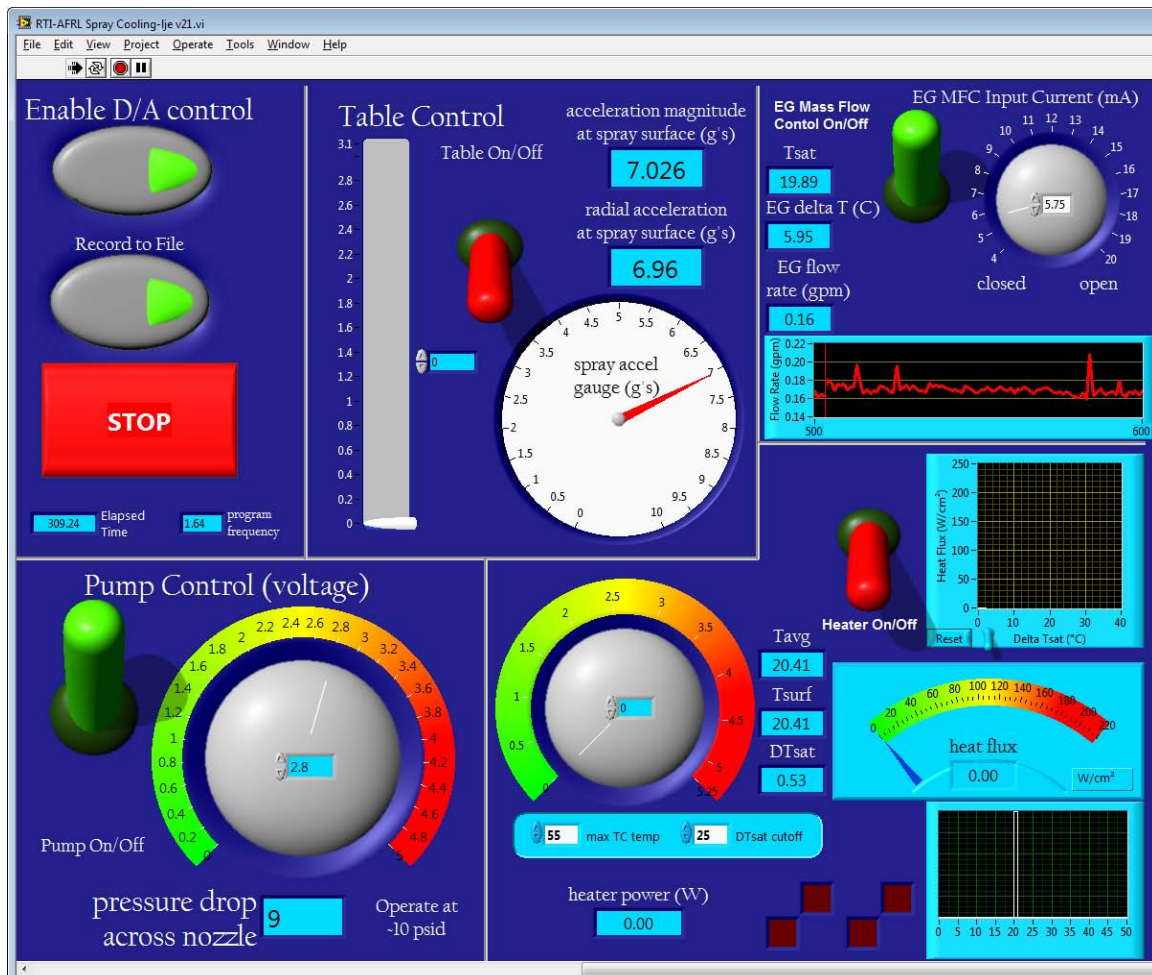


Figure G-1 RINI Centrifuge ESC Control Screen.

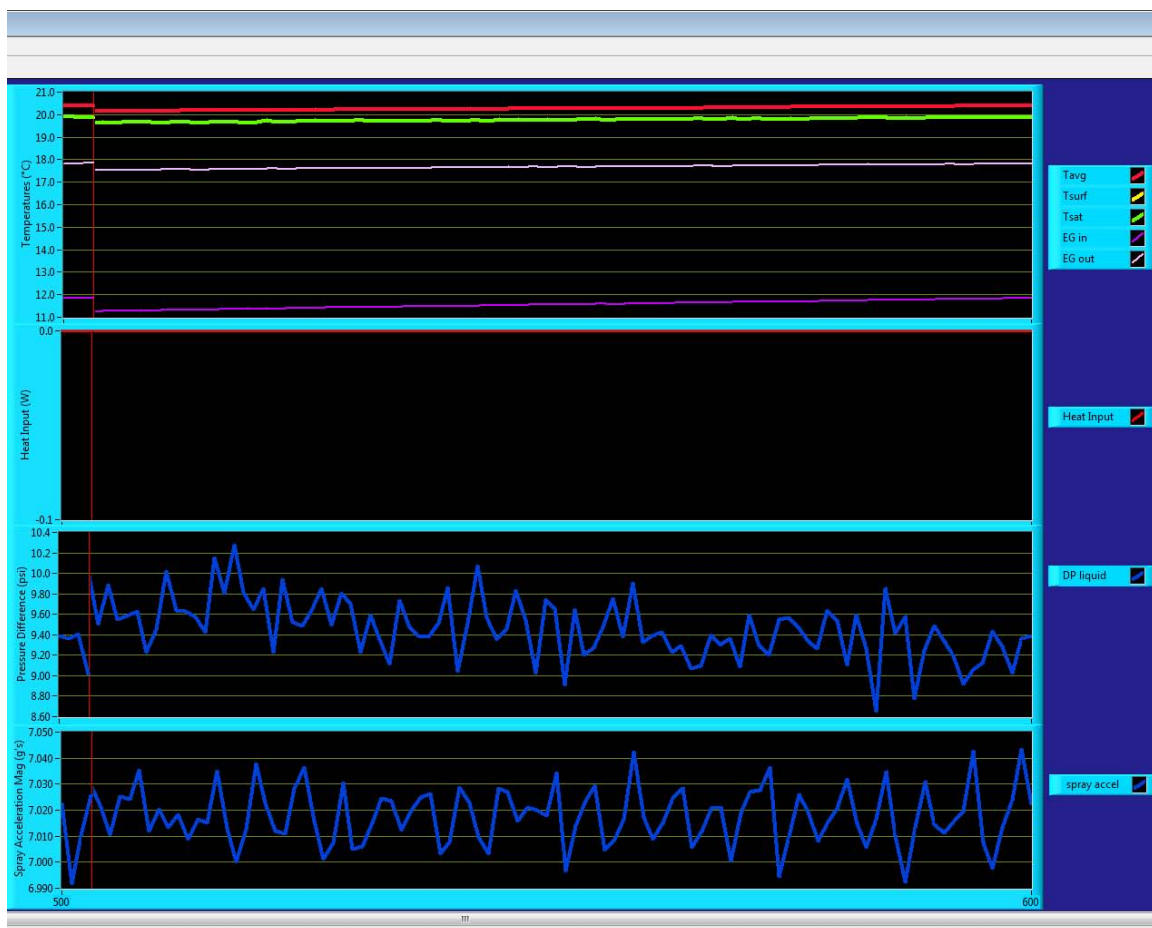


Figure G-2 RINI Centrifuge ESC Strip Chart and Steady State Screen.

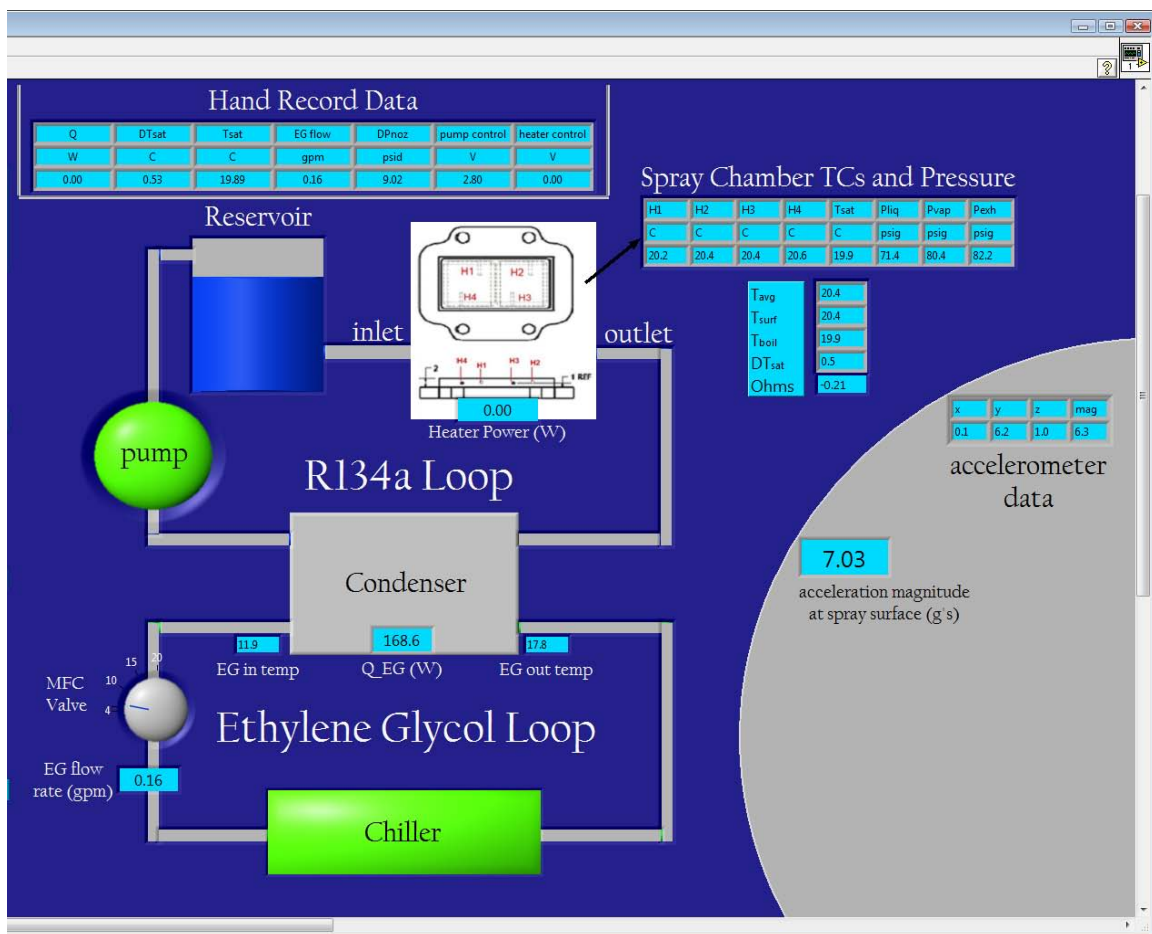


Figure G-3 RINI Centrifuge ESC Flow Loop and Hand Record Data Screen.

After all data is collected in a .txt format, it will be converted to an Excel (.xlsx) file format for further data reduction.

G11.0 REPORTING REQUIREMENTS

Upon completion of data collection, AFRL/RZPS (in collaboration with RINI) will generate a Technical Report detailing the experimental setup, testing, and results.

G12.0 OTHER PROGRAM UNIQUE RESOURCE REQUIREMENTS

This test activity does not have any other program unique resource requirements.

G13.0 TECHNICAL RISK ASSESSMENT

Although equipment failure is unlikely, the nature of the testing imparts unusual stresses on OEM components (pumps, transducers, etc.). The largest portions of technical risk are related to uncertainty (e.g. variation in heater power and measurements due to slip rings, convection effects due to high velocity in air, etc.).

G14.0 SAFETY

The testing has been approved by AFRL/SE (Thanh Chu) with the safety documentation appended.

G15.0 SECURITY

The only security requirements are those associated with safety. The centrifuge test cell must stay closed during spin testing to avoid injury. The precautions taken to this end are: locked side door, warning beacon, and closed main door with “Test In Progress” sign affixed that would need to be removed to enter the test cell. No other security requirements are necessary.